The Astrophysical Journal, 629:797–815, 2005 August 20

THE VERTICAL STELLAR KINEMATICS IN FACE-ON BARRED GALAXIES: ESTIMATING THE AGES OF BARS

D. A. Gadotti[1] and R. E. de Souza
Departamento de Astronomia, Universidade de São Paulo, Rua do Matão, 1226 Cidade Universitaria CEP, 05508-090, São Paulo SP, Brazil; dimitri@astro.iag.usp.br, ronaldo@astro.iag.usp.br
Received 2004 September 17; accepted 2005 April 28

ABSTRACT

In order to perform a detailed study of the stellar kinematics in the vertical axis of bars, we obtained high signal-to-noise spectra along the major and minor axes of the bars in a sample of 14 face-on galaxies and used them to determine the line-of-sight stellar velocity distribution, parameterized as a Gauss-Hermite series. With these data, we developed a diagnostic tool that allows one to distinguish between recently formed and evolved bars, as well as to estimate their ages, assuming that bars form in vertically thin disks that are recognizable by low values for the vertical velocity dispersion σ_z. Through N-body realizations of bar unstable disk galaxies we were also able to check the timescales involved in the processes that give bars an important vertical structure. We show that σ_z in evolved bars is roughly 100 km s^{-1}, which translates to a height scale of about 1.4 kpc, giving support to scenarios in which bulges form through disk material. Furthermore, the bars in our numerical simulations have values for σ_z generally smaller than 50 km s^{-1}, even after evolving for 2 Gyr, suggesting that a slow process is responsible for making bars as vertically thick as we observe. We verify theoretically that the Spitzer-Schwarzschild mechanism is quantitatively able to explain these observations if we assume that giant molecular clouds are twice as concentrated along the bar as in the rest of the disk.

Subject headings: galaxies: bulges — galaxies: evolution — galaxies: formation — galaxies: kinematics and dynamics — methods: *n*-body simulations

1. INTRODUCTION

In the last 10 years or so, bars have gradually become much more than just an intriguing dynamical curiosity (as in the pioneering studies of, e.g., Toomre 1963, 1964; Kalnajs 1972), so that attention has now shifted to the major role they play in the formation and evolution of galaxies. Contributions to this change of perspective came from various different kinds of analysis, including the realization that bars may induce the formation of spiral arms and rings (e.g., Schwarz 1981; Combes & Gerin 1985; Buta 1986; see also Buta & Combes 1996), involving the transfer of angular momentum to the outer parts of the galaxy and resulting in an accumulation of gas in the central regions (e.g., Athanassoula 1992a, 1992b; Friedli & Benz 1993, 1995; Sakamoto et al. 1999a, 1999b), sweeping large-scale chemical abundance gradients (Martin & Roy 1994; Zaritsky et al. 1994), possibly building a reservoir of active galactic nucleus (AGN) fuel (Shlosman et al. 1989, 1990) and provoking central bursts of star formation (e.g., Sérsic & Pastoriza 1965, 1967; Carollo et al. 1997; Gadotti & dos Anjos 2001). Moreover, a number of works developed a new bulge-building scenario in which bars play a fundamental role (e.g., Combes & Sanders 1981; Kormendy 1982; Kormendy & Illingworth 1983; de Souza & dos Anjos 1987; Pfenniger & Norman 1990; Combes et al. 1990; Balcells & Peletier 1994; Kuijken & Merrifield 1995; Norman et al. 1996; Courteau et al. 1996; Peletier & Balcells 1996; Berentzen et al. 1998; Merrifield & Kuijken 1999; Bureau & Athanassoula 1999, 2005; Athanassoula & Bureau 1999; see also the recent review by Kormendy & Kennicutt 2004).

In spite of the undisputed relevance of bars in the evolution of galaxies and even though one of the major concerns of any physical science is to measure timescales for natural phenomena, we are not aware of any directed and systematic study of the ages of bars. Areas in which such work might have a substantial impact include the models of Bournaud & Combes (2002), in which bars may be destroyed and rebuilt a few times in a Hubble period, the polemic and long-sought correlation between the presence of bars and AGNs in galaxies (e.g., Mulchaey & Regan 1997; Ho et al. 1997a, 1997b; Knapen et al. 2000; Laine et al. 2002; Crenshaw et al. 2003; Laurikainen et al. 2004), the debated frequency of bars at higher redshifts (van den Bergh 2002; Sheth et al. 2003, and references therein; see also Elmegreen et al. 2004; Jogee et al. 2004), and obviously the formation history of galactic bulges.

To estimate how long a bar has been evolving in a specific galaxy, one essentially has to measure its vertical extent. This follows from the fact, first shown by Combes & Sanders (1981), that when bars form in disks, they are vertically thin, while the onset of vertical resonances rapidly causes them to become thicker in this direction. It is also possible that the hose instability (Toomre 1966; Merritt & Sellwood 1994), which occurs whenever the velocity dispersion in the vertical direction is 3 times smaller than it is in the plane of the disk, also plays its role in this context by raising the vertical extent of the stellar orbits in the bar region. It is now generally agreed that these processes are likely responsible for the existence of the so called boxy-peanut bulges (see Bureau & Freeman 1999). The age signature of bars can thus be acquired from studying the kinematics along their vertical axis, since it is by elevating the velocity dispersion in this direction that bars evolve and grow away from the plane of the disk.

Another issue that must be discussed in this context regards the difficulties encountered by what until recently has been the standard scenario for bar formation in trying to explain the existence of bars in galaxies of such early type as lenticulars (see,

[1] Current address: Laboratoire d'Astrophysique de Marseille, 2 Place Le Verrier, 13248 Marseille Cedex 4, France.

TABLE 1
Basic Data for All Galaxies in Our Sample

Name (1)	Type (2)	D_{25} (3)	log R_{25} (4)	m_B (5)	cz (6)	AGN (7)	Companion (8)
NGC 1302	SB0(r)	3.89	0.02	11.40	1730	...	N
NGC 1317	SABa(r)	2.75	0.06	11.85	1941	...	Y
NGC 1326	SB0(r)	3.89	0.13	11.42	1365	LINER	N
NGC 1387	SAB0(s)	2.82	0.00	11.82	1328	...	Y
NGC 1440	SB0(rs)	2.14	0.12	12.58	1504	...	N
NGC 2665	SBa(rs)	2.04	0.13	12.96	1740	...	N
NGC 4314	SBa(rs)	4.17	0.05	11.22	963	LINER	N
NGC 4394	SBb(r)	3.63	0.05	11.53	772	LINER	Y
NGC 4579	SABb(rs)	5.89	0.10	10.68	1627	LINER/Sey1.9	N
NGC 4608	SB0(r)	3.24	0.08	11.96	1823	...	N
NGC 4984	SAB0(rs)	2.75	0.10	11.80	1243	...	N
NGC 5383	SBb(rs)	3.16	0.07	12.18	2226	...	Y
NGC 5701	SB0/a(rs)	4.26	0.02	11.82	1556	LINER	N
NGC 5850	SBb(r)	4.26	0.06	12.04	2483	...	N

Notes.—Cols. (1) and (2) show, respectively, the name and the morphological type of the galaxy, while col. (3) shows its diameter in arcminutes at the 25 B magnitude isophotal level, and col. (4) shows the decimal logarithm of its major to minor axes ratio at the same level. Cols. (5) and (6) show, respectively, the apparent B magnitude and the radial velocity in km s^{-1}. All these data were taken from de Vaucouleurs et al. (1991, hereafter RC3). Col. (7) presents an AGN classification according to the NASA Extragalactic Database (NED). In col. (8), "Y" means that there is a companion galaxy similar in size physically interacting within 10′, while "N" means that there are no companion galaxies. To make this analysis we used RC3 and the Lyon Extragalactic Data Archive (LEDA).

e.g., Gadotti & de Souza 2003 and references therein). As the velocity dispersion of the stars in the disk rises, the galaxy becomes more and more stable against bar formation through disk instability. Moreover, the presence of a conspicuous bulge also inhibits this instability (Toomre 1981; Sellwood & Moore 1999). However, Athanassoula (2003) shows that the unresponsive rigid halo used in older numerical experiments led to a false conclusion, namely, that a dark matter halo prevents the onset of the bar instability in the interior disk. In reality, the opposite is true: the exchange of angular momentum between disk and halo particles in fact produces even *stronger* bars and might even be a necessary ingredient to account for the existence of barred lenticulars. Other authors have introduced additional critical details that were not considered previously and these are briefly discussed in later sections.

In this paper, we obtain suitable stellar kinematical parameters to develop a diagnostic tool that enables us to estimate the ages of bars in a sample of 14 face-on galaxies. In § 2, we present the sample and the observations done, while in § 3 we show how the kinematical parameters were determined and introduce our method for bar age estimates. Our results are presented in § 4. To numerically assess the timescales involved in the vertical growth of bars and in this way to gain a deeper understanding of their evolution, several N-body simulations were performed. The results of these are presented in § 5, along with a brief discussion of bar-forming scenarios. In § 6, we discuss our results, also considering some of the possible implications for our present knowledge about bar formation and evolution. Finally, § 7 summarizes the paper by presenting our main conclusions. We used a value for the Hubble constant of $H_0 = 70$ km s^{-1} Mpc^{-1}.

2. SAMPLE AND OBSERVATIONS

Relevant properties of the galaxies in our sample are shown in Table 1. While all of them are bright face-on galaxies in the local universe, one can see that our sample spans a variety of galaxy morphologies. Of the 14 objects, there are 10 strongly barred galaxies and 4 weakly barred ones. Moreover, 7 are of types S0 or S0/a, 3 are type Sa, and there are also 4 Sb galaxies. Also, our sample contains 4 galaxies with an identified companion that may be gravitationally interacting and 5 with nonstellar nuclear activity. This variety is helpful in trying to evaluate clues related, for instance, to the prominence of the bulge, bar strength, and the gravitational perturbation of a companion. The presence of galaxies with active nuclei might also be relevant to understanding the role played by bars in the fueling of this phenomenon.

In Figure 1 we show images of all the galaxies in our sample. Lines displayed horizontally show the extent to which our spectra were taken along the bars' major and minor axes. For instance, one can see that in the case of the SB0 galaxy NGC 4608, the spectra along the bar minor axis are all within the bar, while those from the SBb galaxy NGC 5850 extend into the region outside the bar, in the disk.

Our spectra were taken in two different sets of observing runs. One in the north, on the nights of 1999 May 7 and 2000 April 9–11 with the 2.3 m University of Arizona Steward Observatory Bok Telescope on Kitt Peak; and the other in the south, on the nights of 2002 March 13 and December 1–5 with the 1.5 m European Southern Observatory telescope at La Silla. The instrumental setups, however, are similar. In all runs we used a Boller & Chivens spectrograph with a spatial resolution of 0.″8 pixel^{-1}, a grating with a dispersion of 1 Å pixel^{-1}, and an instrumental spectral resolution of 1.1 Å, giving a velocity resolution of 65 km s^{-1} in the spectral region of the Mg I feature at 5175 Å, which is approximately the center of all spectra taken. The differences between the north and south spectra are the slit width (2.″5 in the north and 2″ in the south), the average seeing (1.″5 in the north and 1.″8 in the south), and the spectral range (typically 1000 Å in the north and 2000 Å in the south).

The north spectra are composed from four 1800 s exposures with the slit oriented along the bar major axis and two 1800 s exposures with the slit positioned along the bar minor axis. In contrast, in the south we have taken, respectively, four 2700 s exposures and two 2700 s exposures, and the slit was always centered on the galaxy nucleus. Thus, the spectra along the bars' minor axes have generally a lower signal-to-noise ratio (S/N) than those along the bars' major axes. This is also due to the fact that the surface brightness decreases more quickly along bars'

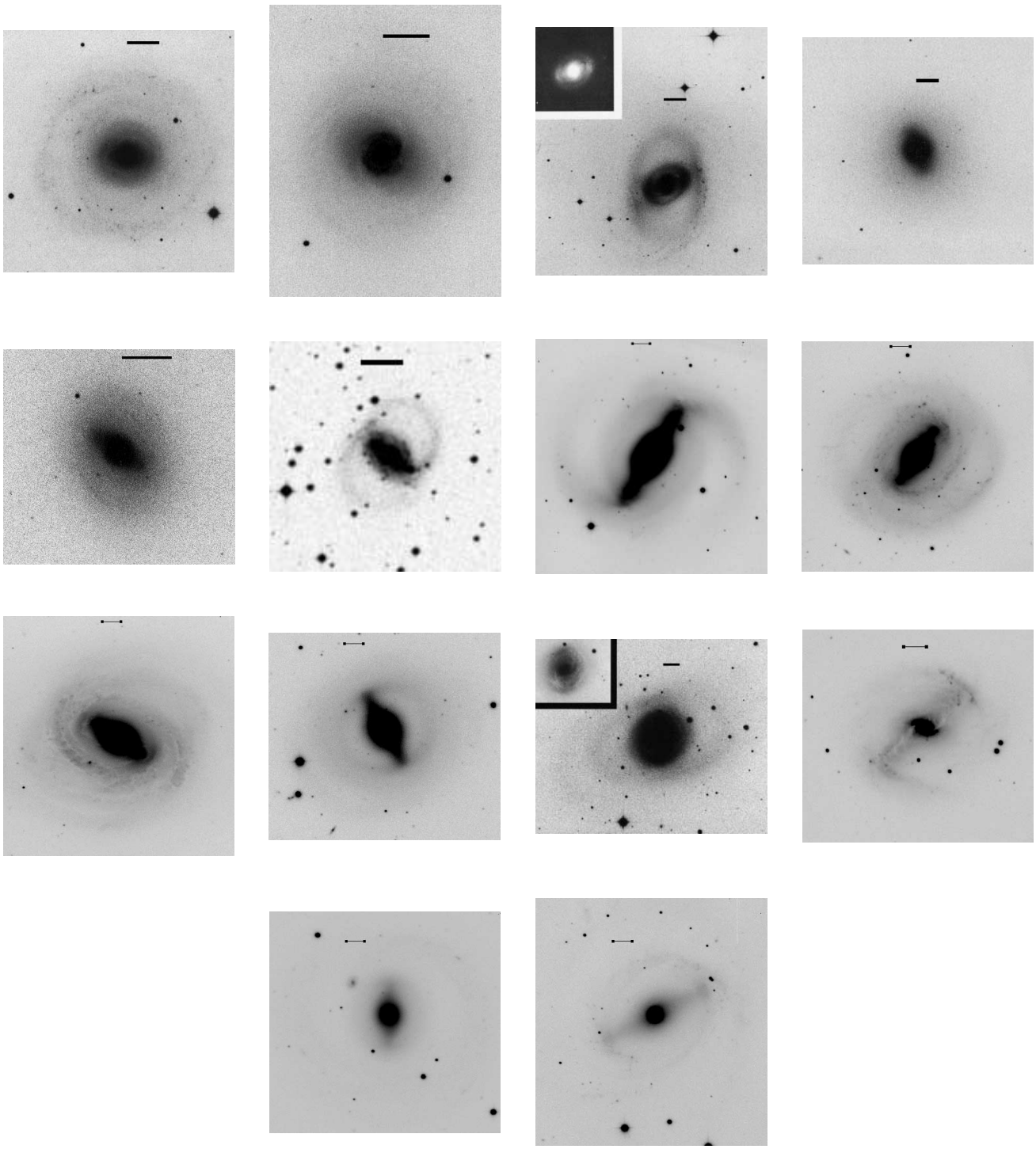

FIG. 1.—All galaxies from our sample. *Left to right and top to bottom*: NGC 1302, NGC 1317, NGC 1326, NGC 1387, NGC 1440, NGC 2665, NGC 4314, NGC 4394, NGC 4579, NGC 4608, NGC 4984, NGC 5383, NGC 5701, and NGC 5850. Horizontal lines in each panel are approximately 20″ in length, except for NGC 2665, for which it is 30″. These images were taken from the Carnegie Atlas of Galaxies (Sandage & Bedke 1994), the Digitized Sky Survey, and from our own *R*-band CCD images (Gadotti & de Souza 2005).

minor axes. Because of the difference in the telescope apertures, the south spectra have also a lower S/N than the north spectra in general, even considering the larger exposure times in the south runs.

We have also obtained spectra for several standard stars in every run. These are standards for spectrophotometry, velocity measurements, and to obtain Lick indices, spanning spectral types from M to O. In the north we observed Feije 34 (spectral type O; Oke 1990), HR 3951 (G3 V), HR 6458 (G0 V), HR 6685 (F2 I), HR 6770 (G8 III), HR 6775 (F7 V), HR 6806 (K2 V), and HR 6868 (M1 III), HD 89449 (F6 IV), HD 90861 (K2 III), HD 92588 (K1 IV), HD 136202 (F8 III–IV), HD 155500 (K0 III), and HD 172401 (K0 III). In the south the stars observed were HR 1544 (A1 V), HR 1996 (O9.5 V), HR 3454 (B3 V), HR 2429 (K1 III), HR 2574 (K4 III), HR 4267 (M5.5 III), HR 4657 (F5 V), HR 4995 (G6 V),

HR 5019 (G6 V), and HR 5568 (K4 V), HD 134439 (K0 V), HD 37984 (K1 III), HD 66141 (K2 III), HD 71597 (K2 III), and HD 92588 (K1 IV). The spectral types are from Hoffleit & Warren (1995).

All spectra were reduced and extracted from the spectral CCD images using the same standard procedures with the `onedspec` and `twodspec.longslit` tasks from IRAF.[2] Dark-current, overscan, and bias were treated as in imaging (e.g., Massey 1997), whereas flat-fielding required some extra care, consisting of a response correction of the dome flat fields to eliminate the continuum from the dome diffuse light and an illumination correction with the twilight sky flat fields (see, e.g., Massey et al. 1992).

To extract the spectra we used the IRAF `kpnoslit.apall` task. To assure that there are no relevant geometric distortions in our instrumental setup, meaning that one single tracing may be used to extract all spectra from the same spectral image, we verified that the dispersion axis is the same along the spatial axis, i.e., that it is parallel in different positions along the slit. For this we have observed the same standard star in six different positions along the slit in a single frame and compared the tracing in all positions. The spectra were extracted for each galaxy along the major and minor axes of the bars in the center and in eight other different positions along the slit length. To minimize the S/N drop in the outer spectra, these were obtained from a gradually larger spatial interval and were centered at $r = 0''$, $2''.05$, $4''.5$, $11''.9$, and $19''.3$ at each side of the center of the galaxy along each bar axis, where r is the galactocentric radius. The full width of these bins is approximately $2''.4$, 4, $7''.2$, $15''.2$, and $21''.6$, respectively. Thus, the spectra at $r = 0''$, $4''.5$, and $19''.3$ are adjacent, i.e., there are no pixels between the bins, although they do not overlap, as are those at $r = 2''.0$ and $11''.9$. But considering the seeing effects the only two pairs of independent spectra are at $r = 0''$ and $11''.9$ and at $r = 2''.0$ and $19''.3$. Because the S/N drops very quickly from the center, it was not possible to obtain spectra farther out.

The spurious contribution from the sky was determined with the light in the outskirts of the slit ($3'$ from the center in the north sample and $2'$ in the south), where the light contribution from the galaxy is much smaller, and subtracted from the data. Emission sky lines that were not eliminated in this step were manually corrected by direct interpolation. This was especially necessary in the north sample due to the proximity of the city of Tucson to Kitt Peak (see Kennicutt [1992], where relevant sky lines over Kitt Peak are presented). Cosmic rays and bad pixels were also removed by statistical means. The extracted spectra were then continuum normalized and calibrated in wavelength. The error in the latter step was verified to be around 10 km s^{-1} in the region of interest (i.e., at about the Mg I feature).

The next and final step was to bring all spectra to the local standard of rest (LSR). This was, of course, first done with the velocity standard stars (with velocities available in Abt & Biggs [1972] and in the Astronomical Almanac), whose corrected spectra were then used to bring the other ones to the LSR. This was done with the cross correlation technique (Tonry & Davis 1979), whereby the availability of spectra from stars of many different spectral types was helpful in minimizing the errors caused by template mismatch. As the S/N per pixel is an essential parameter in calculating the errors in the derived line-of-sight velocity distributions (LOSVDs), they were determined for every galaxy spectrum. We found that S/N $\sim 40-50$ in the central regions of the galaxies, while it drops to $\sim$10–20 in the outermost spectra.

[2] IRAF is distributed by the National Optical Astronomy Observatory, which is operated by the Association of Universities for Research in Astronomy, Inc., under cooperative agreement with the National Science Foundation.

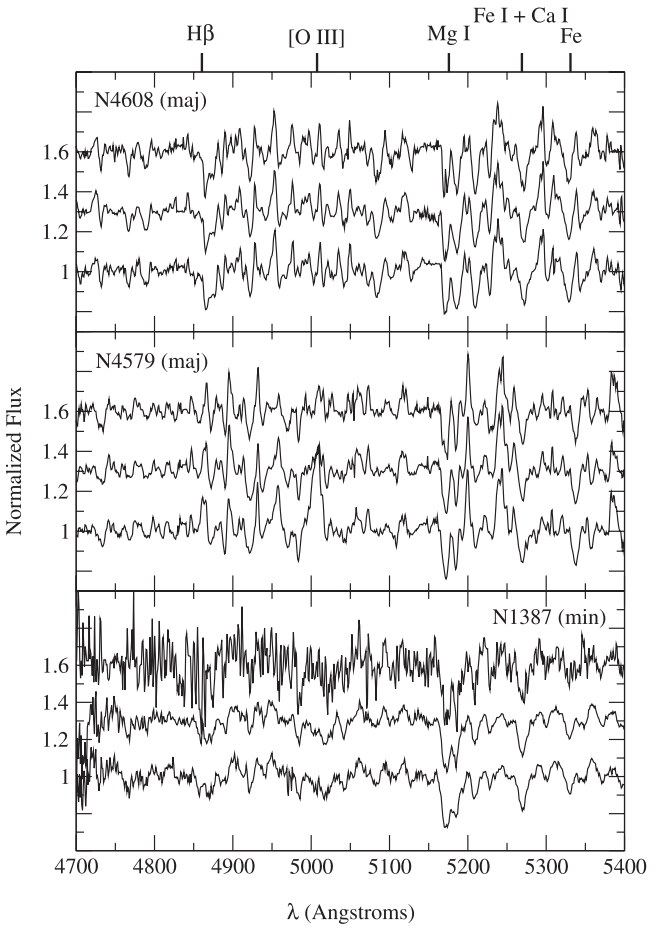

FIG. 2.—Some typical examples of the spectra we obtained. The top two panels refer to spectra obtained along the bar major axis of NGC 4608 and NGC 4579, both from the north sample. The bottom panel shows spectra obtained along the minor axis of the bar in NGC 1387 from the south sample. For each galaxy, as indicated, the bottom spectrum is the central one, while the middle one was extracted at $4''.5$ from the center and the top one at $19''.3$. The latter were artificially dislocated in this figure to avoid crowding. The emission line at $\lambda \approx 5200$ Å in NGC 4579 is the [N I] doublet.

In Figure 2 we show some illustrative examples of the spectra obtained. The two top panels refer to spectra obtained along the bar major axis of NGC 4608 and NGC 4579, both from the north sample. The bottom panel shows spectra obtained along the minor axis of the bar in NGC 1387, from the south sample. It is worth noticing how the higher values for σ_z in the latter produce a larger width in, e.g., the Mg I lines and the Hβ and [O III] emission lines in the LINER/Seyfert 1.9 galaxy NGC 4579, which are particularly strong in the center, as expected.

3. KINEMATICAL PARAMETERS AND BAR AGE ESTIMATES

3.1. *Determining the LOSVDs*

The method we have chosen to determine the LOSVDs with our data is line profile–fitting in the pixel space through a Gauss-Hermite series (van der Marel & Franx 1993). In this case, assuming, as is generally done, that the main difference between the spectrum of a galaxy and that of a suitable template star is due to the stellar velocities in the galaxy (see, e.g., Binney & Merrifield 1998), following a distribution close to Gaussian,

one may write the line profile in the galaxy spectrum as a function of the line-of-sight stellar velocity v, as

$$L(v) = \frac{\gamma\alpha(w)}{\sigma}\sum_{j=0}^{4} h_j H_j(w), \tag{1}$$

where

$$\alpha(w) = \frac{1}{\sqrt{2\pi}} e^{-w^2/2} \tag{2}$$

and

$$w \equiv \frac{v - v_0}{\sigma}. \tag{3}$$

In these equations, γ is the parameter that adjusts the line depth, σ is the stellar velocity dispersion (in our case, $\sigma \approx \sigma_z$), v_0 is the average radial velocity of the system (in our case, $v_0 \approx 0$), h_j represents numerical constants, and $H_j(w)$ are the orthogonal Hermite polynomials (see Abramowitz & Stegun 1965). We may rewrite equation (1) as

$$L(v) = \frac{\gamma\alpha(w)}{\sigma}[1 + h_3 H_3(w) + h_4 H_4(w)], \tag{4}$$

where

$$H_3(w) = \frac{1}{\sqrt{6}}\left(2\sqrt{2}w^3 - 3\sqrt{2}w\right) \tag{5}$$

and

$$H_4(w) = \frac{1}{\sqrt{24}}\left(4w^4 - 12w^2 + 3\right), \tag{6}$$

as we have truncated the Gauss-Hermite series in the terms of order 4 (higher order terms are not retrieved reliably, in general), and since $h_0 = H_0(w) = 1$ and $h_1 = h_2 = 0$ (see van der Marel & Franx 1993).

Thus, to derive the kinematical parameters along the vertical axis in the major and minor axes of the bars of the galaxies in our sample, we have developed an algorithm that can accommodate template spectra of up to five different stars to determine γ, v_0, σ, h_3, and h_4 from the galaxy spectrum. However, to optimize efficiency we have used only up to three different template stars, verifying that in our case the addition of more stars would not result in a significant improvement in the quality of the results. In this way, errors from template mismatch are severely reduced (see, e.g., Rix & White 1992), as our code is also able to determine the contribution of each stellar type to the galaxy spectrum that maximizes the quality of the fit (i.e., minimizes the χ^2-value). As shown by van der Marel & Franx (1993), this method minimizes the correlation between the errors in the different kinematical parameters that determine the line profile, which makes error evaluation more secure. Moreover, these authors also show that the method is less sensitive to template mismatch, as the line profile can be fit into the small differences of the spectral properties of the template stars and the galaxy by adjusting the higher order moments of the Gauss-Hermite series. Hence, the relevant kinematical parameters we have determined for each galaxy spectrum obtained are σ_z and the third- and fourth-order moments of the LOSVD parameterized as Gauss-Hermite series, h_3 (the skewness of the velocity distribution) and h_4 (its kurtosis). This was done twice for each spectrum, since we also parameterized the LOSVDs with pure Gaussians, i.e., with $h_3 = h_4 = 0$ to check the consistency of our results.

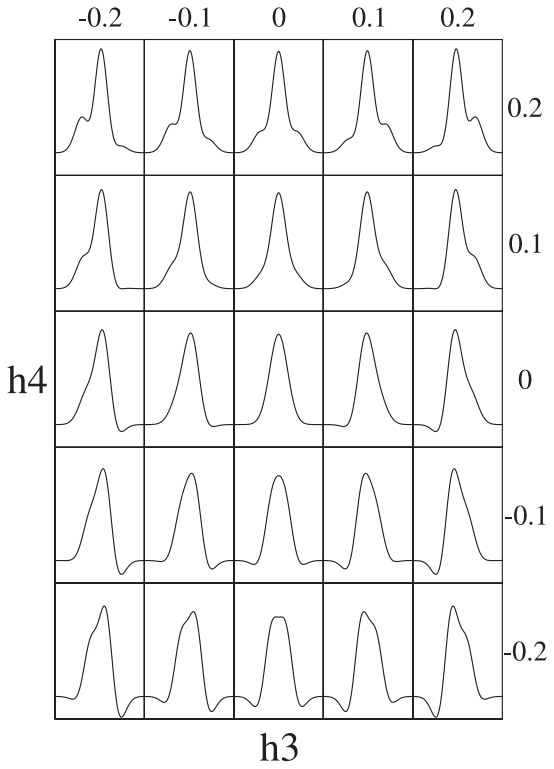

FIG. 3.—A pure Gaussian ($h_3 = h_4 = 0$) may suffer asymmetric deviations when $h_3 \neq 0$ and symmetric deviations when $h_4 \neq 0$.

Figure 3 illustrates how h_3 and h_4 modify the shape of the distribution. As can be seen, h_3 is responsible for asymmetric deviations. A negative value for h_3 means that there is an excess of stars whose velocities are lower than the average system velocity, while the opposite, of course, is true for a positive h_3. This is why an anticorrelation between h_3 and v in edge-on galaxies is generally found to be a signature of a cold, rapidly rotating system (Fisher 1997; Chung & Bureau 2004). On the other hand, a nonnegligible h_4 introduces symmetric deviations. A negative value for h_4 indicates a higher number of stars with line-of-sight velocities close to the average velocity, making the LOSVD pointy, whereas a positive value is a sign that the distribution is wider near the average velocity. Note also that typically h_3 and h_4 are very small, in the range -0.1 to 0.1, and that to retrieve reliable values for these parameters the S/N in the spectrum must be higher than about 50. This means that a meaningful discussion of these deviations in our work can only be undertaken in regard to the central spectra. Even so, however, it is evident that using a generalized Gaussian (Gauss-Hermite series) to parameterize the LOSVDs maximizes the quality of the fit and the reliability of the values of the kinematical parameters.

To certify that our code is able to produce reliable estimates, a series of tests was performed. In these tests, a stellar spectrum was artificially redshifted and widened by a known LOSVD, resulting in an artificial galaxy spectrum, with a spectral resolution of 1 Å and a S/N equal to 30 to match the typical characteristics

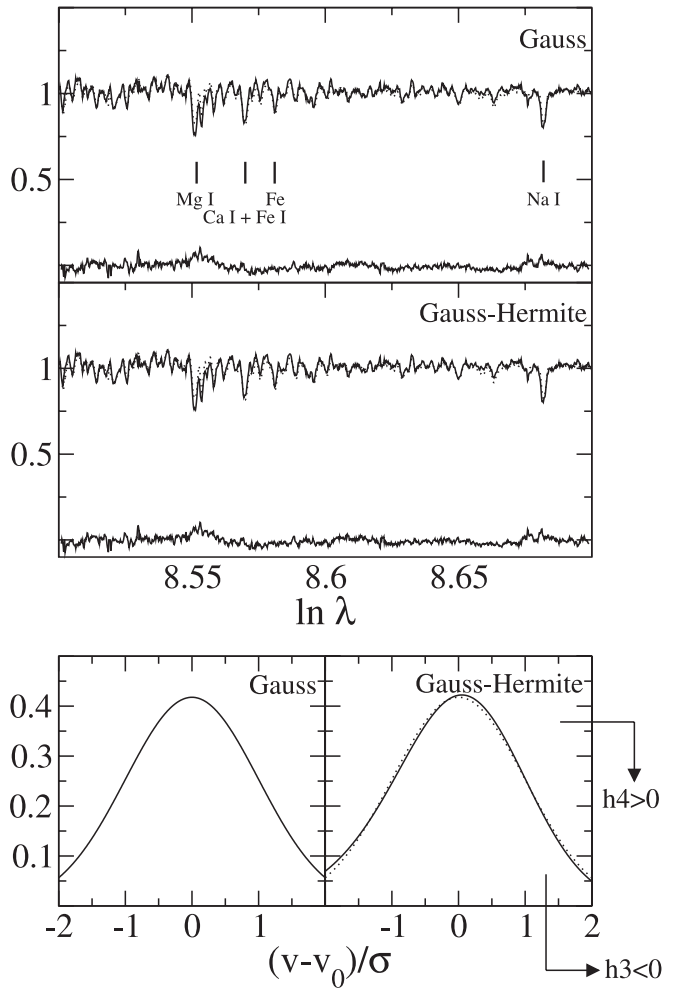

FIG. 4.—Example of the fits generated by our code to retrieve the LOSVDs from the galaxy spectra, in this case NGC 1302 at 2″.0 from the center along its bar major axis. The results from the two parameterizations are shown: the velocity distribution as a pure Gaussian (*top, and bottom left*) and as a generalized Gaussian (Gauss-Hermite series; *middle, and bottom right*). The top and middle panels show the galaxy spectrum (*solid line*) and the solution found with the template stars and the determined LOSVD (*dotted line*). Residuals are also shown. The bottom panels show the determined LOSVDs. Note the effects of the higher order moments of the generalized Gaussian. In the bottom right panel the dotted line is a pure Gaussian profile for comparison.

of the spectra in our sample. For the tests we generally chose K giant stars whose spectra were taken from the Elodie archive, which contains high-resolution spectra for many stars (see Prugniel & Soubiran 2001). We then used our algorithm to retrieve the LOSVD from the synthetic galaxy spectrum using the stars for which we have obtained the spectra as a template. The results have been always excellent: the solution found by our code, i.e., the template spectrum dislocated and widened by the determined LOSVD has always been very similar to the original synthetic galaxy spectrum. In any case, every LOSVD determined in in this work has been carefully checked to verify that the solution found is indeed similar to the real galaxy spectrum. To clarify this procedure, Figure 4 shows an example of the fits to the spectrum of NGC 1302 produced by our code at 2″.0 from the center along its bar major axis. Note, moreover, that, to avoid infinite values for v, our code truncates it, following the relation $\langle v_e^2 \rangle = 4\langle v^2 \rangle$, where v_e is the escape velocity in virialized systems (see Binney & Tremaine 1987).

It is worth noting how we selected the template stars in the running of our code to determine the LOSVDs. We followed a careful criterion to minimize even further errors from template mismatch. For every galaxy spectrum we first ran the code using a single stellar template spectrum. This was done with all stars observed under the same instrumental setup. The star that provides the best fit, i.e., lower χ^2, is the first star selected. After that, we ran the code again using as template spectrum a combination of the spectra from the first selected star and all of the other remaining stars separately. Initially, this combination is an average of both stellar spectra, but the algorithm is able to give weights to each spectra in order to achieve better results. Again, the pair of stars that produces the best fit is selected. Finally, the algorithm is applied once again, using the spectra of the stellar pair selected combined with the spectrum of each of the remaining stars, to determine the third suitable template star in the same fashion. Generally, with three stars we have achieved the best χ^2, but in some cases using only two stars produced better results. Only one set of template stars was used to retrieve the LOSVDs from all spectra of a given galaxy, since we have verified that the best set of stars does not change when we run the code for spectra taken at different galactocentric distances.

Another cause of uncertainties from template mismatch involves the chemical abundances of the template stars. Although most of the template stars we use are K giants or similar, their metallicity (the [Fe/H] ratio) compared to the solar value ranges from −0.62 (HR 6775) to +0.25 (HR 3951) in the north and from −1.92 (HD 134439) to +0.07 (HR 2429) in the south, using the estimates in Cayrel de Strobel et al. (2001). Although we did not find the necessary data in the literature, this likely means that our template stars also span a significant range in the [Mg/Fe] abundance ratio. This obviously plays a role in studies like ours in which Mg and Fe lines are used to calculate the kinematical parameters. This should be suitable to account for differences in the abundance of the galaxies and the stellar templates. Interestingly, following our scheme to choose the most suitable template spectra, stars with [Fe/H] values too different from solar were not considered suitable by our code. For instance, in the north sample the two most frequently chosen stars were HR 6806 ([Fe/H] ≈ −0.30) and HR 3951, and in the south sample these were HD 37984 ([Fe/H] ≈ −0.55) and HR 2574 ([Fe/H] ≈ −0.16), with no significant or systematic differences according to whether galaxies are early or late type. In fact, one should expect such a result, as our measurements concern mostly the central regions of galaxies whose morphological types are also mostly early.

The spectral region used to measure the kinematical parameters of the galaxies in our sample is the one that contains mostly absorption lines from the photosphere of, typically, K giant stars in the range from, approximately, the Mg I triplet at $\lambda = 5175$ Å to the Na I feature at $\lambda = 5893$ Å. This region also includes relevant lines in this respect, such as the Fe I + Ca I lines at $\lambda = 5265$ Å and the Fe lines at $\lambda = 5328$ Å. In a significant part of the cases studied here a narrower spectral range was used that excludes the Na I feature. The Hα and [Hβ] lines, at 6563 and 4861 Å, respectively, were excluded from the analysis to avoid spurious results from the complicated emission from gas. In the case of galaxies with active nuclei, emission lines such as [O III] (5007 Å) were automatically excluded from the analysis by our code, which ignores lines that are too discrepant in the galaxy and template spectra. Nonetheless, we mention a potential source of uncertainty in the spectra of galaxies that present a strong [N I] emission line (the doublet at 5198, 5200 Å), such as NGC 4579 (see Fig. 2). As shown by Goudfrooij & Emsellem (1996), this feature may affect the line-strength measurements of

the Mg I triplet. Three other galaxies in our sample show also this [N I] emission line: NGC 2665, NGC 4984, and NGC 5701. Although they are LINERs, the spectra of NGC 1326 and NGC 4314 present only a small feature, while in that of NGC 4394 we have not detected the line. Inspecting our results, we find no clear systematic trends regarding this issue.

3.2. *The Ages of Bars*

Having measured the value of σ_z along the major and minor axes of the bars in our galaxy sample, we are ready now, as a first-order approach, to distinguish recently formed and evolved bars. But before going on, let us discuss what one expects to find. We argue that to make this distinction one has to rely not only on the value of σ_z in the bar but also on its radial behavior in both axes, since the contribution from the bulge and the disk must also be considered. As stellar systems supported by pressure, bulges will, in general, contribute to a rise in the stellar velocity dispersion in the center, irrespective of the bar age. On the other hand, since in some cases the outer spectra along the bar minor axis extend into areas where we are essentially measuring the value for σ_z without relevant contributions from the bar and the bulge (i.e., the vertical velocity dispersion in the disk), in these cases a comparison between the values of σ_z in the bar and in the disk is most valuable. It should also be kept in mind that a significant variation in the velocity dispersion from galaxy to galaxy (even those with similar morphological types) is expected.

Delhaye (1965; see also Binney & Merrifield 1998) estimates that $\sigma_z \sim 15$ km s^{-1} in the solar neighborhood for K giant stars. In general, similar values are found for other spectral types. The velocity dispersion in the radial, σ_r, and azimuthal, σ_φ, directions are, respectively, $\sim$30 and $\sim$20 km s^{-1}. In fact, in the Galactic disk, typically, $\sigma_z/\sigma_r \sim 0.5$ and $\sigma_\varphi/\sigma_r \sim 0.6$, and thus $\sigma_r > \sigma_\varphi > \sigma_z$. As the bar length in the Galaxy is estimated to be around 3 kpc (Blitz & Spergel 1991; Merrifield 2004) and also considering the study of stellar orbits in disk potentials (Binney & Tremaine 1987), these values are expected to be representative for the outer disk in late-type spiral galaxies (Sb–Sc). As the velocity dispersion in the disk rises inward (van der Kruit & Searle 1981), at a galactocentric distance of about the disk length scale h, which is 3.5 ± 0.5 kpc in the Galaxy, $\sigma_z \sim 30$ km s^{-1}. Typical values for σ_z in the center of this class of galaxies are around 50 km s^{-1} (Bottema 1993). For lenticular galaxies, $\sigma_z \sim$ 100 km s^{-1} in the center, including the contribution from the bulge (McElroy 1995). Farther out, $\sigma_z \sim 50$ km s^{-1} in lenticulars (Fisher 1997).

We can also make an evaluation of the relation between σ_z and the height scale in the disk. In the epicycle approximation (Binney & Tremaine 1987), the vertical oscillation of the stars in the disk in cylindrical coordinates (r, φ, z) is given by $\ddot{z} = -\nu^2 z$, where ν is the epicycle vertical frequency, given by

$$\nu^2 = \left(\frac{\partial^2 \Phi}{\partial z^2}\right)_{(r,z=0)}, \tag{7}$$

where Φ is the disk gravitational potential. Moreover, in a highly flattened system

$$\frac{\partial^2 \Phi}{\partial z^2} = 4\pi G\rho(r,\ z). \tag{8}$$

And thus

$$\nu^2 = 4\pi G\rho(r,\ z = 0). \tag{9}$$

This means that ν depends only on the mass density in the plane of the disk and that in a recently formed bar, assuming that bars are a global dynamical disk instability, the stars are oscillating with this vertical frequency. For the Galaxy, in the solar neighborhood, $\nu = (3.2 \pm 0.5) \times 10^{-15}$ s^{-1}.

On the other hand, through the reasonable assumption that ν is independent of z, we have

$$z = z_0 \sin(\nu t + \phi_0), \tag{10}$$

where z_0 is the disk height scale, t is time, and ϕ_0 is a phase constant. This implies that

$$v_z = \dot{z} = z_0 \nu \cos(\nu t + \phi_0) \tag{11}$$

and

$$\langle v_z^2 \rangle = \sigma_z^2 = \frac{1}{2} z_0^2 \nu^2. \tag{12}$$

Thus, considering the disk of the Galaxy typical,

$$z_0 = \frac{\sqrt{2}\sigma_z}{\nu} = 215\left(\frac{\sigma_z}{15 \text{ km s}^{-1}}\right) \text{ pc}. \tag{13}$$

Edvardsson et al. (1993) show that for the thin disk of the Galaxy $\sigma_z = 18$ km s^{-1}, while $\sigma_z = 39$ km s^{-1} for the thick disk. Following our equation (13), this means that z_0 is, respectively, 258 and 559 pc. Hence, stars with low σ_z indeed belong to the disk, whereas values of σ_z as high as about 100 km s^{-1}, which implies in $z_0 \approx 1.4$ kpc, are certainly not related to the disk component. It is interesting to note that these results are in agreement with the quasi constancy of z_0 along galactic disks (de Grijs & Peletier 1997; van der Kruit 2002). But note also that the radial rise in z_0 is more expressive in the disks of early-type spirals.

Thus, as we have just shown, by measuring σ_z we can have a direct estimate of the vertical extent of the disk. A recently formed bar, as being part of the disk, still has the kinematical properties that characterize disks, namely a low velocity dispersion, that produces a vertically thin structure, which we can infer by observing low ($\lesssim$50 km s^{-1}) σ_z values. As the bar evolves, the already mentioned processes like vertical resonances and the hose instability give the bar a higher vertical extent by raising σ_z. These processes, however, make no changes in the remaining of the disk.

In this way, we are able now to devise prescriptions that will make us able to distinguish between recently formed and evolved bars. The first one is possible if one has measurements of σ_z in the bar and in the disk outside the bar and the bulge. This was possible for a few cases in this study, where the outer spectra taken along the minor axis of the bar reach areas in the disk where the light from the bar and the bulge makes only a small contribution. By comparing the velocity dispersion in the bar and in the disk, a recently formed bar will have yet disk kinematics, whereas an evolved bar will have a larger σ_z than the disk. In Figure 5 we show schematically how this comparison may be

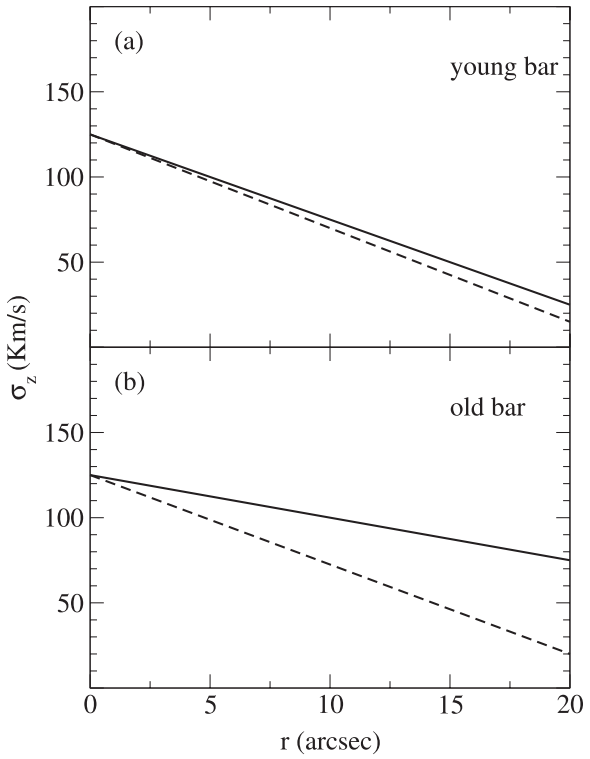

FIG. 5.—If one is able to measure σ_z not only along the bar major axis (*solid line*) but also in the bar minor axis (*dashed line*), reaching in the latter case regions in the galaxy dominated only by the disk, i.e., outside the contributions from the bulge and the bar, then a simple comparison of the values of σ_z in the bar and in the disk will suffice to evaluate if the bar is young or old. A young bar (*a*) has a velocity dispersion yet similar to the one in the disk, whereas an evolved bar (*b*) has a much higher σ_z than the disk due to its dynamical evolution. Note that the units for the abscissae are of course only meant to represent our study. The location of the different σ_z behaviors will clearly vary in different galaxies.

done. The top panel is an example of a recently formed bar, while the bottom one shows the signature of an evolved bar.

Since obtaining kinematical data for the fainter parts of the disk of galaxies is very telescope time demanding, in most of the cases the outer spectra taken along the bar axes are still within the bar or the bulge, even considering the minor axis. Thus, we often may not have an estimate of σ_z in the pure disk to compare to the one in the bar. Hence, we expect that a young bar has not only a low σ_z but also that its radial profile shows a steep outward fall, as the bulge in the center has a much hotter kinematics. Figure 6*a* shows schematically what would be the expected signature of such a case. On the other hand, an old bar is dynamically hotter than the disk and is possibly as hot as the bulge, and in such case the σ_z radial profile is somewhat flat (see Fig. 6*d*). However, we may expect to find cases in which the bulge contribution may be misleading. Especially for late-type galaxies, whose bulges may be substantially dynamically colder than average, even a young bar may display a fairly flat σ_z profile, as we show in Figure 6*b*. Furthermore, for the early-type galaxies with their very hot bulges, an evolved bar may show up a steep σ_z profile as can be seen in Figure 6*c*.

Having set up the prescriptions to distinguish young and old bars we postpone to §§ 5 and 6 the further step of evaluating how much older than young are evolved bars. Instead, in the next section we present the results obtained with the spectra taken in this study.

4. RESULTS

The σ_z radial profiles along the bar major and minor axes of the galaxies in our sample are shown in Figures 7 and 8 for the south and north samples, respectively. The reason for a few empty panels in these figures is that we unfortunately were not able to make measurements along the minor axis of the bars in NGC 4984 and NGC 5383. Although we do not present and discuss our results concerning h_3 and h_4, since the errors on these number estimates render them too unreliable, the fact that similar results are obtained from both parameterizations (i.e., pure Gaussian and Gauss-Hermite series) is encouraging. In order to properly analyze these profiles and try to evaluate which bars are young and which are not, it is also important to know over which radial range the bulge dominates the emitted light and where the light is dominated by the bar or the disk, whose kinematics we want to measure. To determine this we used the Aladin interactive sky atlas (Bonnarel et al. 2000) with optical images publicly available through NED. As estimates like these are somewhat subjective we did not try to establish them too precisely. Nonetheless, these estimates indeed serve our goals. Also, the values referring to the bulge, in particular, denote where its light dominates over that from the bar (and hence the measured kinematics) rather than its actual

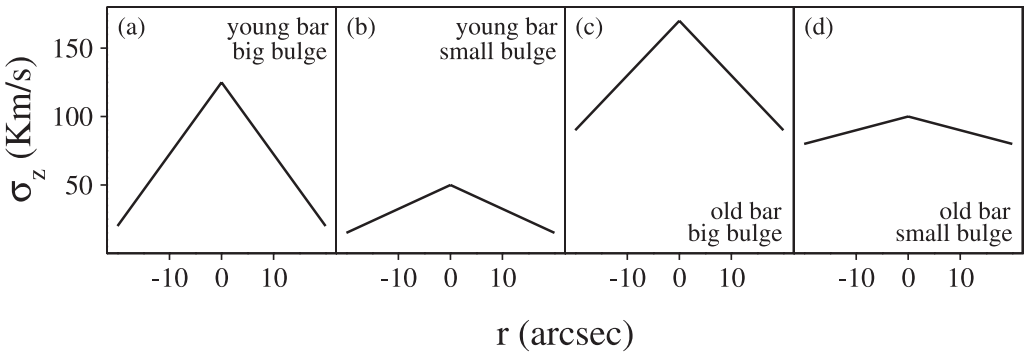

FIG. 6.—Typical radial profiles of σ_z for young and old bars in the presence of a bulge. In most cases, the acquisition of spectra from pure disk regions is very difficult and even the outermost spectra along the minor axis may be still within the bar. In these cases the radial behavior of σ_z is somewhat similar along both the major and minor axes of the bar. The kinematics of the bulge basically affects the central velocity dispersion. The two leftmost panels show examples of recently formed bars, revealed by the low values for σ_z typical of disk stars, while in the rightmost panels the evolved bars may be recognized by values of σ_z that can not be ascribed to a disk. In (*a*) and (*c*), however, the bulge is dynamically hotter than the bar, even an evolved one. In (*b*) and (*d*), on the other hand, the kinematics of the bulge and the bar are similar, and this may be true for a young or for an old bar. Morphological differences may also account for this different behaviors, as bulges of earlier type galaxies have a larger velocity dispersion. Note that the units for the abscissae are of course only meant to represent our study. The location of the different σ_z behaviors will evidently vary in different galaxies.

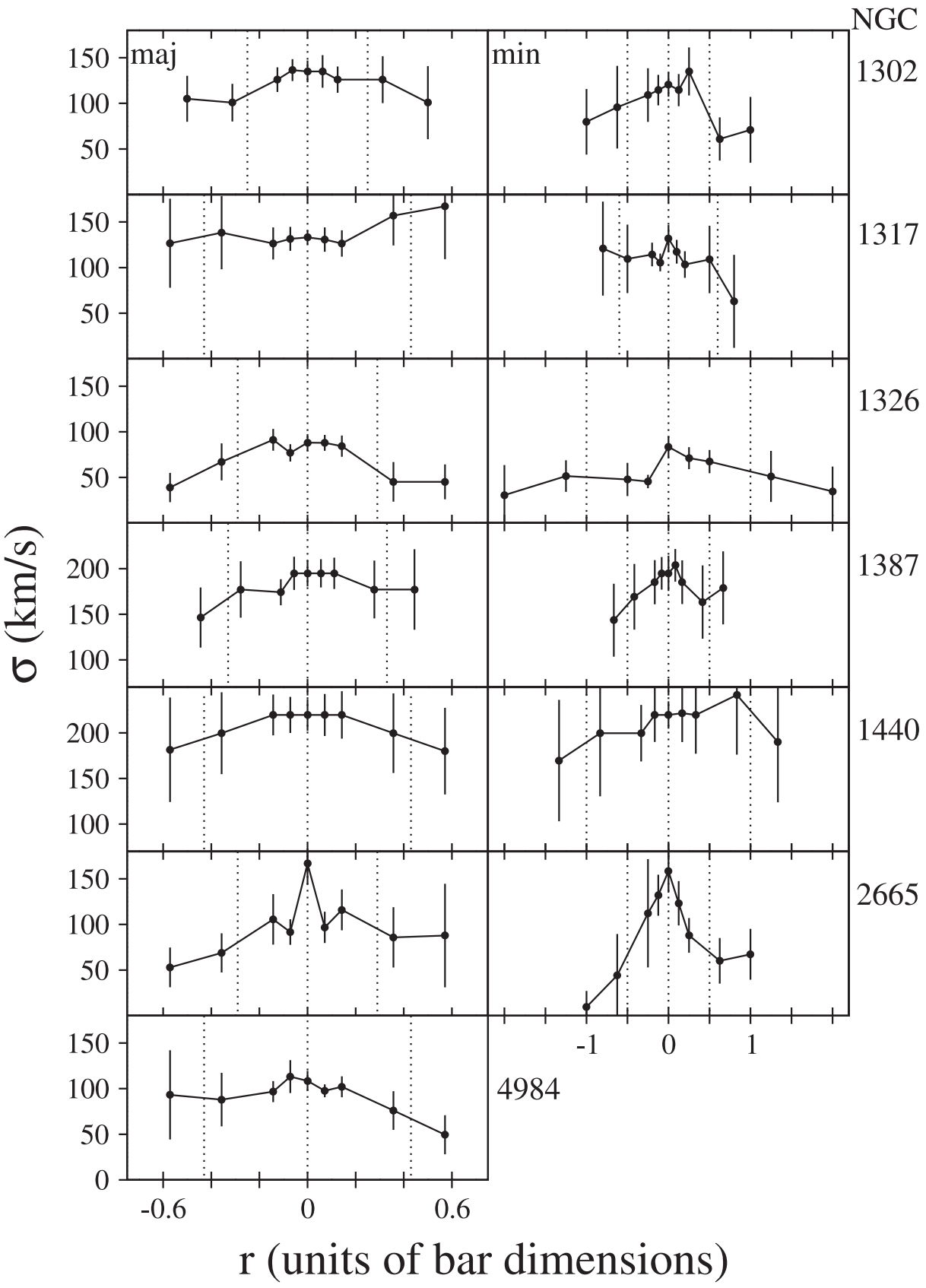

FIG. 7.—Vertical velocity dispersion radial profiles for the galaxies in our south sample along the major and minor axes of the bars, as displayed. The figures refer to a parameterization of the LOSVDs as a pure Gaussian, but similar results were obtained when we made use also of the h_3 and h_4 higher order moments of the Gauss-Hermite series. Dotted lines mark the center and the region where the emitted light is dominated by the bulge. Units in the abscissae are normalized by the bar semimajor and semiminor axes.

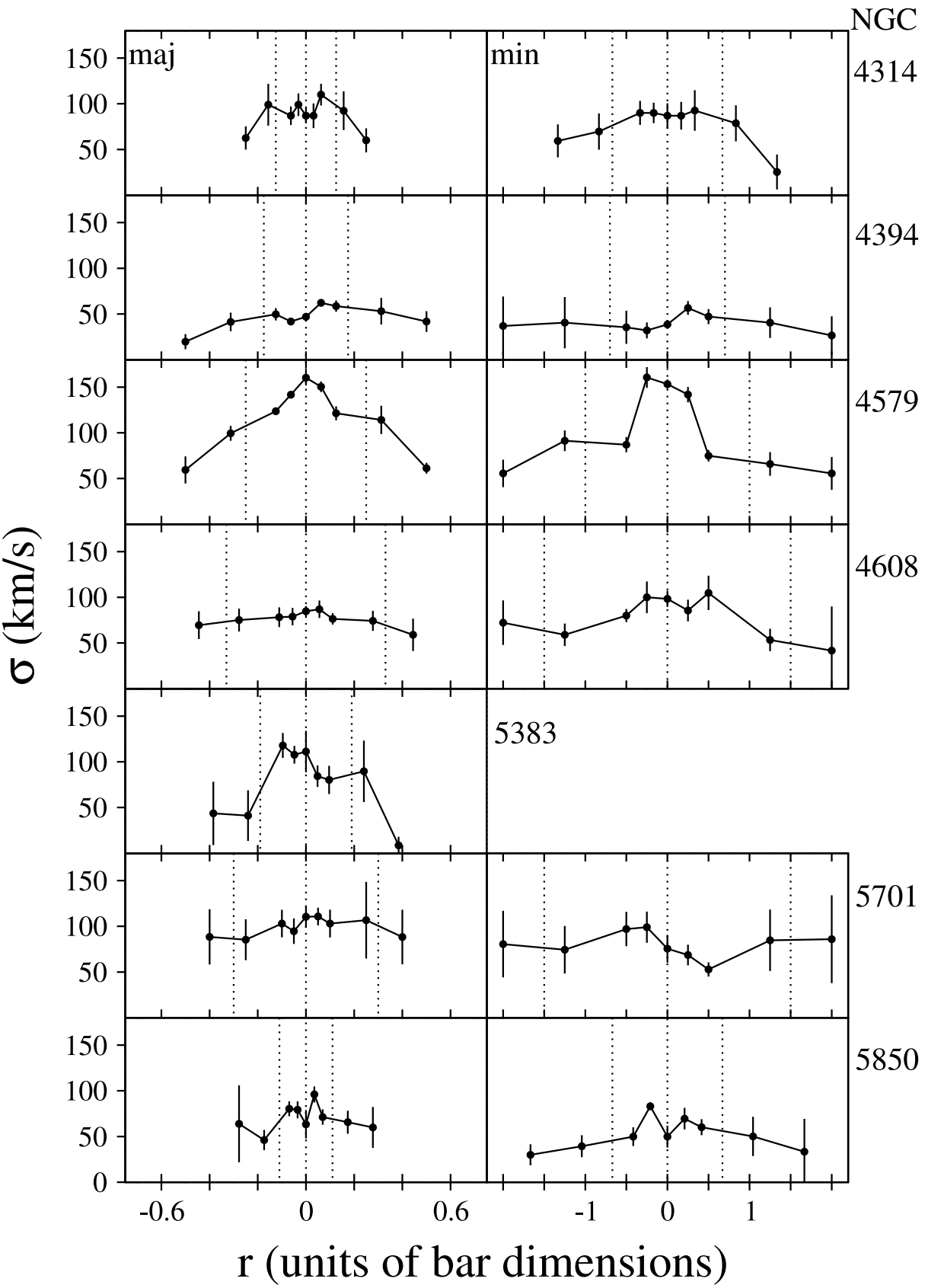

FIG. 8.—Same as Fig. 7, but for the north sample.

TABLE 2
PROPERTIES OF BULGES AND BARS OF THE GALAXIES IN OUR SAMPLE[a]

Galaxy (NGC) (1)	Bulge Major Axis (2)	Bar Major Axis (3)	Bulge Minor Axis (4)	Bar Minor Axis (5)	$\sigma_{z,\mathrm{bar}}$ (km s^{-1}) (6)	$\Delta\sigma_z$ (km s^{-1}) (7)	Error (1) (km s^{-1}) (8)	Error (2) (km s^{-1}) (9)	Bar Age (10)
1302	10	40	10	20	100	28	47	12	Old
1317	15	35	15	25	145	57	71	70	Old
1326	10	35	10	10	38	8	34	6	Young
1387	15	45	15	30	159	2	52	46	Old
1440	15	35	15	15	178	2	83	20	Old
2665	10	35	10	20	67	32	43	66	Young?
4314	10	80	10	15	59*	20	21	32	Old?
4394	7	40	7	10	28	0	27	23	Young
4579	10	40	10	10	57	6	20	3	Young
4608	15	45	15	10	62	9	38	35	Old
4984	15	35	...	...	68	...	...	...	...
5383	10	52	...	...	23*	...	...	...	Young
5701	15	50	15	10	85*	5	52	7	Old
5850	8	72	8	12	60*	33	40	4	Old

NOTES.—Col. (1) gives the NGC number of the galaxy, while cols. (2) through (5) show the apparent length in arcseconds of the semimajor and semiminor axes of bulges and bars after visual inspection (see text for details). Note that our measurements reach approximately 20″ from the center. Col. (6) gives the vertical velocity dispersion measured along the bar major axis at ≈50%–60% of the bar semimajor length, except when the asterisk indicates that our spectra do not reach this galactocentric distance. Col. (7) gives the difference between cols. (6) and σ_z measured in the disk along the bar minor axis at the same galactocentric distance. The values in cols. (6) and (7) are averages from both sides of the bar axes. Cols. (8) and (9) show error estimates in the values of $\Delta\sigma_z$ according to two different procedures (see § 4). Finally, col. (10) shows whether the galaxy harbor an young or and old bar according to the method and criteria developed here. Doubtful cases are indicated by a question mark.

[a] These are the properties relevant to a proper evaluation of the bar ages from the radial profiles of the vertical velocity dispersion (Figs. 7 and 8).

length.[3] The results are shown in Table 2. Note that our measurements along the bar major axis are always within the bar itself and that the bulge dominates typically the inner 10″–15″ along both axes. We stress also that since the spectra are extracted from ever increasing radial bins (from the center outward), there is some overlap in radius that makes the transitions between the bulge and the bar and sometimes the disk smoother than in reality.

Following the discussion done so far and in view of the results in Figures 7 and 8 it is possible to qualitatively assess bar ages and distinguish between young and old ones. A quantitative approach, however, is highly desirable. Ideally, for this task one would like to have measurements of the stellar vertical velocity dispersion in the disk and in the bar free from *any* light contamination from other structural components, especially the bulge. In this case, a simple comparison between the values of σ_z would reveal how much the bar has vertically evolved from the original disk. Although this is feasible with the slit configuration we used, it is virtually impossible with 2 meter class telescopes, since this means obtaining high-S/N spectra from very faint parts of galaxies. Nevertheless, with the data presented here we can pursue such an endeavor if we carefully take into account the bulge contribution to the recorded light, using our estimates in Table 2. In addition, let us define a fiducial value that represents σ_z in the bar as the average of our farthest measurements along the bar major axis, which for the majority of our galaxies corresponds to ≈50%–60% of the bar semimajor axis length, $\sigma_{z,\mathrm{bar}}$ (col. [6] in Table 2). This choice comes from a compromise between minimizing bulge contamination and considering the galactocentric distances our spectra reach. Similarly, we can define a fiducial σ_z-value for the disk. Since galactic disks generally have a gradient in velocity dispersion, we choose to take the disk fiducial σ_z at the same galactocentric distance from which $\sigma_{z,\mathrm{bar}}$ is defined. Only in this way can a meaningful comparison of both values be achieved. Obviously, however, the disk velocity dispersion is taken along the bar *minor* axis, and the galactocentric distance chosen corresponds to about 1 to 2 times the bar semi-*minor* length. Again, we took an average of our measurements at both sides of the center. Column (7) in Table 2 shows the difference between this and $\sigma_{z,\mathrm{bar}}$, defined as $\Delta\sigma_z$. Hence, with the help of $\sigma_{z,\mathrm{bar}}$ and $\Delta\sigma_z$ we can make a more quantitative assessment in order to distinguish young and old bars.

Then, according to our line of reasoning, some clear cases can be identified. One can say with a certain degree of confidence that NGC 1326, NGC 4394, and NGC 5383 harbor recently formed bars. Their results resemble what we would expect based on Figures 5*a* and 6*a* (for NGC 1326 and NGC 5383) and Figure 6*b* (for NGC 4394). Moreover, $\sigma_{z,\mathrm{bar}} < 40$ km s^{-1} and $\Delta\sigma_z <$ 10 km s^{-1} (although we do not have this parameter for NGC 5383), which in fact point to these bars as still being a vertically thin structure belonging to the plane of the disk.

Clear instances of evolved bars are the ones in NGC 1302, NGC 1317, and NGC 5850. Their σ_z radial profiles resemble Figures 5*b* and 6*d*. These galaxies have $\sigma_{z,\mathrm{bar}} = 100$, 145, and 60 km s^{-1}. The latter value is clearly much lower, but this is a result of the fact that NGC 5850 is of a later morphological class than the former galaxies. In fact, $\Delta\sigma_z \geq 30$ km s^{-1} in the three cases, an indication that these bars have grown vertically from their parent disks.

With these clear instances we can identify typical values for $\sigma_{z,\mathrm{bar}}$ and $\Delta\sigma_z$ in old and young bars. For the recently formed bars the average of $\sigma_{z,\mathrm{bar}} \approx 30$ km s^{-1}, whereas this value climbs to ≈100 km s^{-1} for the evolved ones. Similarly, $\Delta\sigma_z \approx 5$ and 40 km s^{-1} for young and old bars, respectively.

Let us go now to the less clear cases. The behavior of σ_z in NGC 1387 and NGC 1440 shows a relatively steep fall from the

[3] Here we have assumed round bulges for the sake of simplicity. The results from a detailed morphological analysis in Gadotti & de Souza (2005) for seven galaxies in our present sample indicate an average for the central bulge ellipticity ≈0.1. Hence, this assumption seems to be fairly reasonable to our purposes.

center outward in both axes, and their $\Delta\sigma_z$ values are low, presumably indicating young bars. However, their values for $\sigma_{z,\mathrm{bar}}$ are too high for young bars. These are certainly vertically thick and evolved bars, resembling the schema of Figure 6*c*. These are typical cases in which the early-type bulge presents a very high velocity dispersion. The low values of $\Delta\sigma_z$ can likely be explained by light contamination in the bar minor axis from the bulge and the bar even at the outermost spectra. In fact, in these cases, we have no reliable data on the velocity dispersion of the disk alone. Moreover, note that in the outer spectra σ_z is as high as $\sim$150 km s^{-1}. It is hard to understand how the global dynamical disk instability alone could be responsible for the bar in these hot disks, even taking into account that a substantial part of this high-velocity dispersion comes from the bulge and the bar. NGC 4608 and NGC 5701 are similar cases. The influence of the bulge and the bar may be causing low values for $\Delta\sigma_z$, but the high values of $\sigma_{z,\mathrm{bar}}$ clearly put these bars in the evolved bin. Their bulges, however, are not as dynamically hot as those of NGC 1387 and NGC 1440, and their σ_z radial profiles resemble Figure 6*d*.

The following cases are more doubtful, and thus the reader should keep in mind that our conclusions on these cases must be treated with caution. NGC 4314 has intermediate values for both $\sigma_{z,\mathrm{bar}}$ and $\Delta\sigma_z$, and we do not reach far out enough along the bar major axis. However, the σ_z radial profiles along the bar minor axis show an estimate of σ_z in the disk substantially lower than those that refer to the bar. Taking this single point into account it seems more appropriate to consider its bar an evolved one. It can in fact be an example in which bar evolution is at an intermediate stage. NGC 4579 has a $\sigma_{z,\mathrm{bar}}$-value closer to that of an evolved bar and a $\Delta\sigma_z$-value typical of a young one. Our farthest measurements, however, clearly indicate that the bar and disk have a similar σ_z, at least in their outer parts, which makes us consider this bar as still recently formed. Contamination from bulge light may again be the cause for the high $\sigma_{z,\mathrm{bar}}$-values. NGC 2665 is a similar case, and the very low and uncertain σ_z estimates in the farthest points along the bar minor axis may be occulting a young bar behind a high value for $\Delta\sigma_z$. In fact, the σ_z estimates along the bar minor axis do not agree in the outermost points from each side of the galaxy center. Good spectra taken at farther galactocentric distances could certainly avoid and clarify these doubtful cases.

Finally, the case of NGC 4984 is the only one for which we could not arrive to a definite conclusion. The dispersion reaches relatively low values but only on one side of the bar. The lack of minor axis spectra also prevents us from reaching a conclusion. Note also that the inner structure of this galaxy is complex (see Fig. 1) and that Jungwiert et al. (1997) suggest that it has a secondary bar possibly almost aligned with the primary. This complexity certainly is reflected in our results.

We performed three different statistical tests within the R environment[4] to check whether the values we obtained for $\sigma_{z,\mathrm{bar}}$ and $\Delta\sigma_z$ for young and old bars in fact point to different objects. An unpaired Student *t*-test gives a 98% probability that what we defined by young and old bars are indeed different populations considering $\sigma_{z,\mathrm{bar}}$. Support for this conclusion comes from Kolmogorov-Smirnov and Wilcoxon (or Mann-Whitney) tests. These tests, however, do not find a significant difference between young and old bars if one considers $\Delta\sigma_z$. As discussed above, the lack of σ_z measurements far out in the disk (away from the bar and bulge light) for several cases in which an old bar is clearly seen from the analysis of $\sigma_{z,\mathrm{bar}}$ is the likely cause of the latter result. On the other hand, it is evident that the results from these tests considering $\sigma_{z,\mathrm{bar}}$ agree with the distinction made here between recently formed and evolved bars. In a later stage it would also be interesting to try to identify intermediate cases. Note that tests like these do not take into account the observational error in each single measurement of, e.g., $\sigma_{z,\mathrm{bar}}$. However, they use the standard deviation from the mean in both samples (in this case, young and evolved bars) to estimate the observational error and then state the statistical significance of the final result, i.e., the difference between the two samples.

In Figures 7 and 8 one can also verify that at least in NGC 4314 and NGC 5850 there is a central drop in the velocity dispersion. Doubtful cases may be NGC 1317, NGC 4394, NGC 4608, and NGC 5701, since the drop, or the constancy, of σ_z is marginally significant. The remaining majority of the cases show a peak instead, which is more commonly observed. This peculiarity has also been noted by Emsellem et al. (2001) in three other cases. This drop may be caused by a recently formed stellar inner disk that originated in the funneling of gas to the center by the bar. In this context, it is noticeable that NGC 4314, NGC 4394, and NGC 5850 indeed present inner disks, a finding we confirm through a detailed structural analysis in Gadotti & de Souza (2005, hereafter Paper II) using the BUDDA code (de Souza et al. 2004).

Many examples of measurements of the stellar velocity dispersion in galaxies can be found in the literature, but we are not aware of a systematic measure of this physical parameter along face-on bars. Nonetheless, comparisons with previous values may be instructive, even if not exactly relative to a similar study. Corsini et al. (2003) made measurements of the stellar velocity dispersion in NGC 4984 in a manner similar to what we present here. A comparison of the results from both studies shows that the estimates are essentially the same. Fisher (1997) shows estimates for the stellar kinematics of lenticular galaxies. One can verify that his measurements are very similar to ours, as his velocity dispersion estimates for, e.g., NGC 3412, NGC 3941, and NGC 4754 (all barred and more or less face-on) range from $\approx$200 km s^{-1} in the center to $\approx$60 km s^{-1} 20″ away from it. NGC 3941 is an interesting case worthy of being explored in more detail. Not considering that his measurements are at an angle to the bar major axis, one could use our analysis to conclude that the bar is evolved, although better estimates for the velocity dispersion in the disk would be necessary for a more clear conclusion. A similar study involving late-type galaxies can be found in Pizzella et al. (2004). Looking at their results for galaxies that are reasonably face-on, we again find measurements similar to ours. This is the case for NGC 210, NGC 3054, NGC 6878, and NGC 7412, whose stellar velocity dispersion ranges from $\approx$150 km s^{-1} in the center to $\approx$50 km s^{-1} 25″ away from it, although we would expect somewhat lower values in the disks of the two latter galaxies. Similar results were found for NGC 488 and NGC 2985 (Gerssen et al. 1997, 2000), and in Bottema (1993) one also finds, for the four face-on galaxies in his sample, estimates similar to ours. If one considers that $\sigma_z/\sigma_\varphi \sim 0.83$, then inspecting the recent measurements of Kregel et al. (2004), one sees that the range in velocity dispersion they observe in the disks in a sample of edge-on late-type galaxies is in agreement with our estimates for both the late-type galaxies in our sample and the early-type ones, whose σ reaches considerably higher values, also in agreement with previous work (see § 3.2).

Table 2 also shows error estimates for $\Delta\sigma_z$. We followed two different methods to determine these errors. In the first one we propagate the error as is usually done in error analysis considering

[4] See http://www.R-project.org.

the errors from the spectrum fitting, i.e., those errors determined in § 3.1 (displayed as error bars in Figs. 7 and 8). In our second method we do not consider the uncertainties in the spectrum fitting but assume that the error in $\Delta\sigma_z$ is the quadratic mean of the differences between the values of σ_z in the bar and in the disk (that are used to calculate $\Delta\sigma_z$) taken at both of sides of the galaxy center. This sometimes leads to smaller errors. This analysis shows that the relative error in $\Delta\sigma_z$ is large, as one would expect given that it is a difference between close numbers, each one already bringing along considerable uncertainty, since they are estimated from faint light. The impact of this uncertainty in our division between young and evolved bars must not be exaggerated, however, since this was done taken also into account $\sigma_{z,\mathrm{bar}}$ and the full σ_z radial profiles.

5. THE VERTICAL THICKENING OF BARS IN *N*-BODY EXPERIMENTS

It is interesting now to compare the results described in the previous section with *N*-body realizations of the evolution of barred galaxies. This is useful, for instance, to establish the timescales involved in the vertical thickening of bars. Previous studies estimate the timescale for the occurrence of the boxy-peanut morphology, likely a consequence of vertical resonances and/or the hose instability, on the order of 1 Gyr (see, e.g., Combes & Sanders 1981; Combes et al. 1990). But a systematic comparison of the vertical velocity dispersion in observations and simulations has not been done yet. In this section we perform simplistic *N*-body experiments on the evolution of pure stellar disks to use as a first-order approach in making this evaluation. A more realistic treatment would involve adding responsive bulge and halo components, which is beyond our present scope. We note, however, that we intend to perform a more thorough and accurate analysis in a future paper. Thus, the results from this section must be treated with caution and tested with more realistic experiments. They are, however, useful to obtain an approximate order of magnitude of the age difference between the young and evolved bars identified above, as well as—and this may be even more important—to attest that measurements of the vertical velocity dispersion along bar and disk are at least qualitatively useful for bar age estimates, as we propose here.

The experiments were done within the NEMO package (Teuben 1995), and the Barnes & Hut (1986) tree code was used for force calculation. We used virial units, in which $G = M = -4E = 1$, where G is the gravitational constant, M is the mass, and E is the total energy of the system. In the runs a constant time step of typically 2×10^5 yr was employed, giving about 10^3 time steps per crossing time in the systems analyzed. The optimal softening parameter suggested by Merritt (1996; see also Athanassoula et al. 2000) for $N = 10^5$, that is, the number of particles we have used typically, is in the range from $\epsilon \approx 0.01$–0.05, and the latter value was used. The intention here is to minimize spurious effects caused by the small number of particles, especially two-body relaxation, which may heat and thicken the disk. Finally, the aperture (or tolerance) angle used was always $\theta = 0.7$.

The simulated disks are made of responsive particles of equal masses and are exponential and isothermal with a constant height scale (Freeman 1970, 1978; van der Kruit & Searle 1981):

$$\rho_d(r,\ z) = \frac{M_d}{4\pi R_d^2 z_0} e^{-r/R_d} \mathrm{sech}^2\,(z/z_0), \qquad (14)$$

where M_d is the disk mass and R_d its length scale. In this case, the Toomre Q parameter, establishing if the disk is unstable to the bar mode instability, is defined in the usual manner:

$$Q \equiv \frac{\sigma_r \kappa}{3.36 G \Sigma}, \qquad (15)$$

where κ is the epicycle frequency of the stellar orbits in the plane of the disk and Σ is the projected mass surface density. Thus, since $Q \propto \sigma_r = 2\sigma_z \propto (\pi\Sigma z_0)^{1/2}$ (see, e.g., van der Kruit 2002), the stability of the disk is set up in the initial conditions for z_0. In some of the experiments, however, we have directly attributed a constant value to Q in the initial conditions, aiming to force the bar instability. In the latter case, is the vertical extent of the disk that is determined as a function of the Toomre parameter. A correction for the asymmetric drift was applied in the disks, assuming the Milky Way disk as typical (see Dehnen & Binney 1998).

Several simulations were run as to mimic the 2 Gyr evolution of stellar disks with properties similar to the Milky Way disk (see Binney & Tremaine 1987; Binney & Merrifield 1998), i.e., a mass $M_d = 6\times10^{10}\ M_\odot$ and length scale $R_d = 3.5$ kpc. The height scale varies in the different experiments in the range $z_0 = 200$–600 pc, which, as discussed above, has a fundamental influence on the disk stability against bar formation. The center of mass and energy variation were typically of the order of 0.3%.

We now discuss, on the basis of one representative experiment (with $z_0 = 450$ pc), the onset of the bar instability in galaxies and the vertical thickening of bars. This fiducial calculation has a Toomre parameter in the initial conditions estimated by equation (15), which decreases continuously from $\approx$3 in the center to $\approx$1 at the outermost radii. Figure 9 displays the evolution of the pure stellar disk in that, as expected, a strong bar develops. This happens after $t = 6\times10^8$ yr and spiral arms also appear in the so-called grand design morphology. The bar weakens after $t = 5\times10^8$ yr but remains for a similar period, then giving way to an oval bulgelike distortion until the end of the simulation after 2 Gyr. The vertical heating of the disk can be seen clearly in the edge-on projection, as well as how the weakening of the bar originates a bulgelike structure, corroborating previous works (see also Debattista et al. 2004). It remains, however, a matter of debate whether bars are robust, perennial galactic components, or may be easy to dissolve with central mass concentrations as a result of their natural evolution (see Shen & Sellwood 2004).

Figure 10 shows the evolution of the rotation curve in our experiment. This was derived through the simulation of long-slit spectroscopy data, using parameters that match the observations we present in § 2 as concerns the slit width and pixel size on the "sky" and the seeing, i.e., spectral and spatial resolution. The same procedures were followed to extract radial profiles of the stellar vertical velocity dispersion along the major and minor axes of the bar, as is presented and discussed below. Note that the rotation velocities reached are low because we are not including the mass contributions of either the bulge or halo. However, the global shape of the rotation curve is similar to what is generally found for real galaxies (e.g., Rubin et al. 1985). Interestingly, although there is no dark matter halo contribution to these curves, they are quite flat: only a hint of a falloff is observed in the second row of panels. This is at least partially explained by the fact that the particle distribution in our disk models is truncated at about 10 kpc, i.e., only $\approx$3 length scales (but see Barnes et al. 2004).

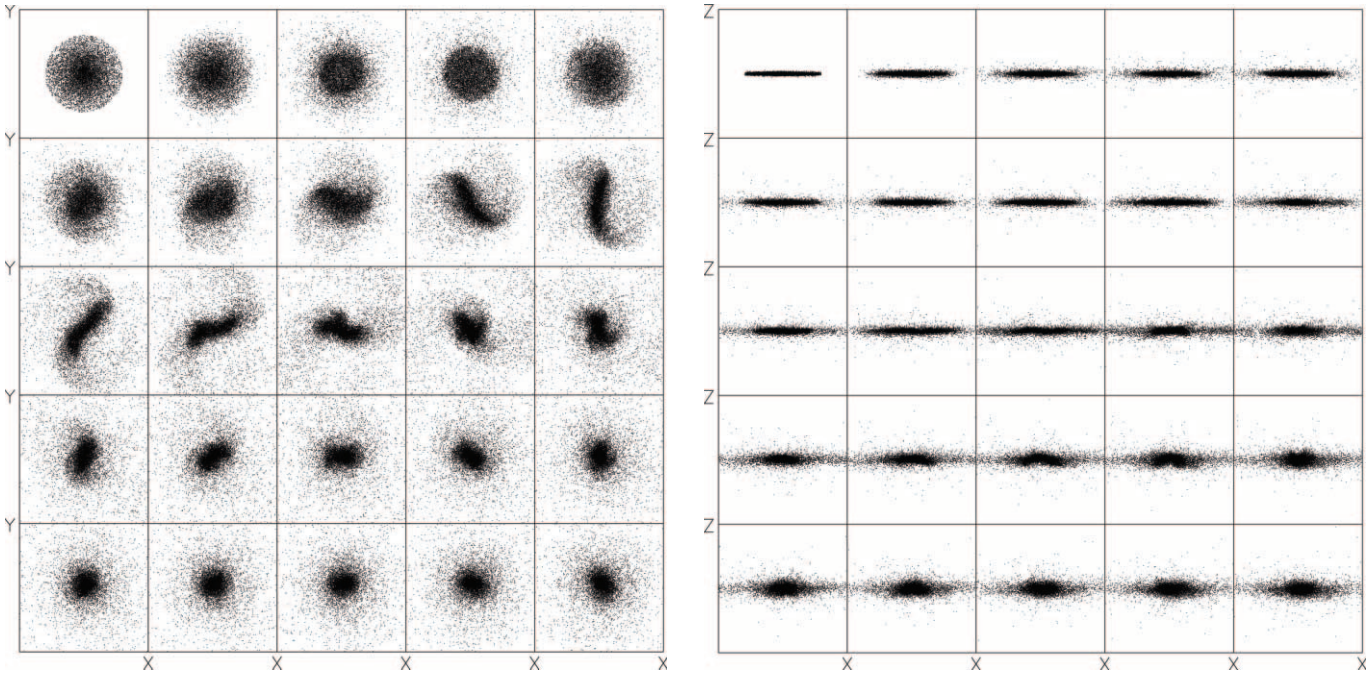

FIG. 9.—Formation of the grand design morphology in the evolution of a pure stellar disk seen face-on (*left*) and edge-on (*right*). The top leftmost panels show the initial conditions, whereas the bottom rightmost panels refer to $t = 1.9$ Gyr of evolution. The time interval between each panel is $t = 8 \times 10^7$ yr, and its physical dimension is 16 kpc. Only 10% of the particles in this simulation are shown.

We have also made some tests with live bulges and rigid halos to realize more complete and realistic systems and verified the difficulties encountered by the old bar formation scenario (based purely on the bar mode disk instability) in explaining the origin of bars in galaxies with kinematically hot disks and conspicuous bulges, as observed in barred lenticulars. However, we can identify five possible ways to salvage the bar mode instability in disks as the origin of bars in galaxies, and these need to be fully explored. First, as shown recently by Athanassoula & Misiriotis (2002) and Athanassoula (2002, 2003), the use of rigid halos is misleading, since their simulations with live halos show that the exchange of angular momentum between the disk and the

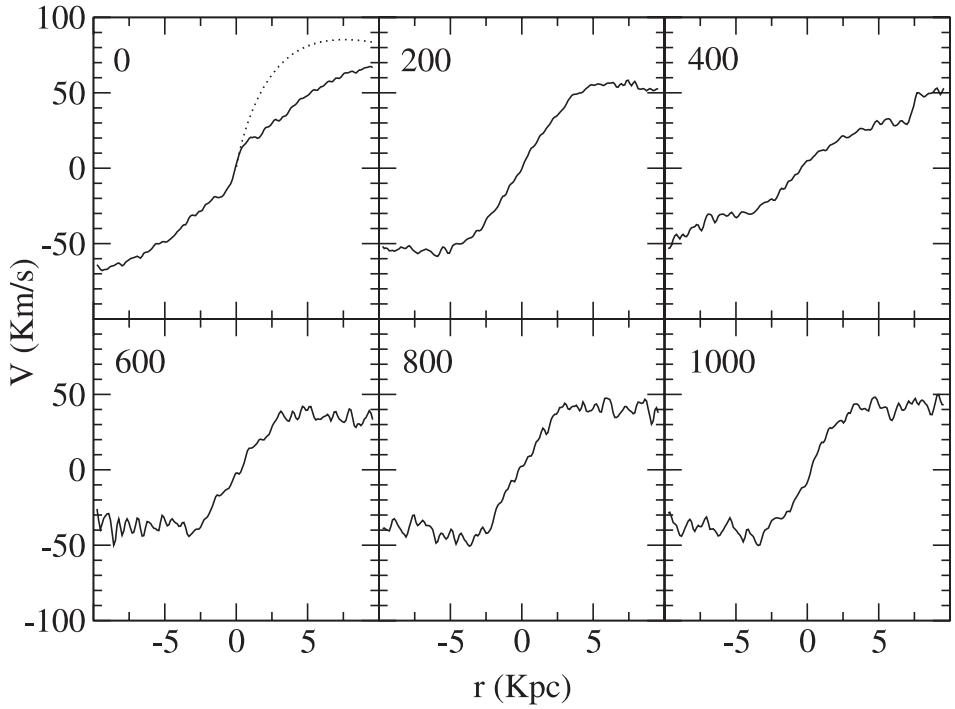

FIG. 10.—Evolution in time of the rotation curve, as measured from simulated long-slit spectroscopy, in our representative stellar disk numerical simulation. The corresponding times in virial units are displayed in the top left of each panel. The last panel corresponds to 2 Gyr of evolution. The dotted line in the first panel is the initial circular speed curve, for comparison.

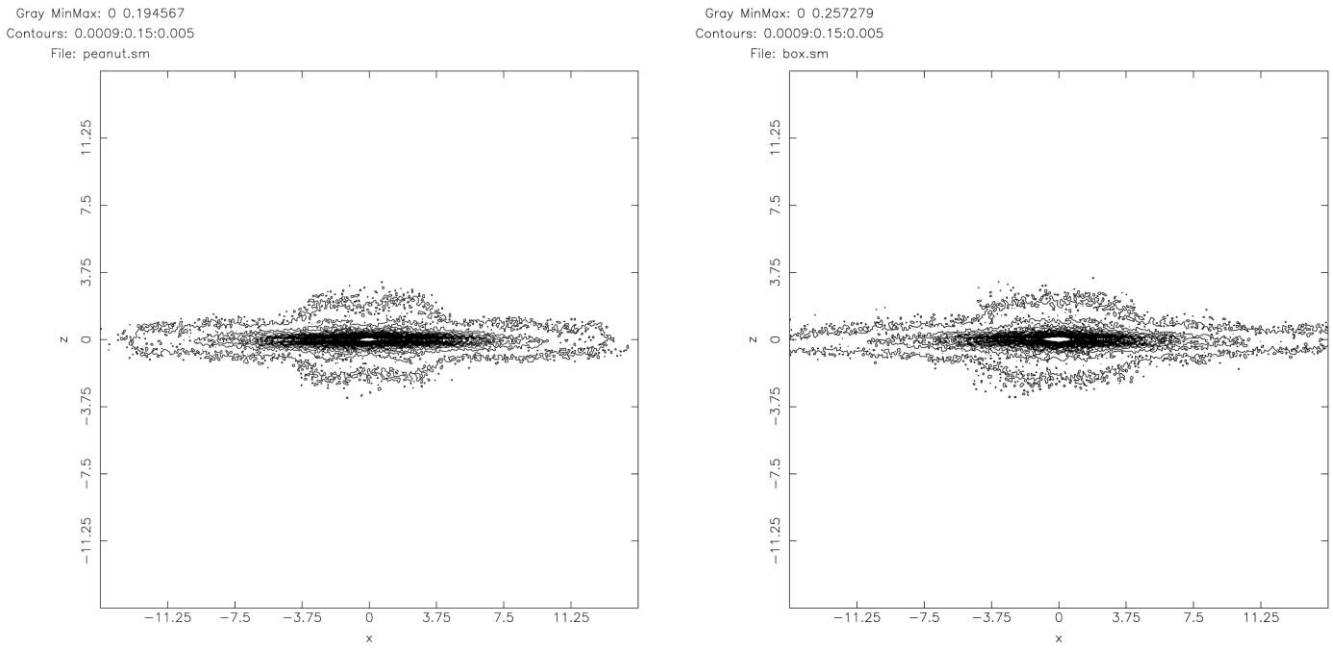

FIG. 11.—Isodensity contours in our fiducial numerical experiment seen edge-on in $t = 3.6\times10^8$ yr (*left*) and in $t = 4\times10^8$ yr (*right*). Note that the peanut morphology appears when the line of sight is closer to a perpendicular orientation with respect to the bar major axis (*left*), whereas the boxy morphology appears when the line of sight is closer to a parallel orientation with respect to the bar major axis (*right*). Dimension units are 650 pc.

halo may, contrary to expectations produced by previous studies, reinforce the bar. Hence, the present standard bar formation scenario adds to the bar mode disk instability the absorption of angular momentum by a responsive halo. Second, as in the scenario of Bournaud & Combes (2002), the infall of gas from the halo in the disk may also create a kinematically cold structure that is bar unstable. Third, as we showed in Gadotti & de Souza (2003), sufficiently eccentric halos can induce bar formation in kinematically hot stellar systems. Finally, we also note that tidal interactions may play a relevant role in this context (Noguchi 2000) and the approach of Polyachenko & Polyachenko (2003).

In all our experiments that do not preclude the appearance of a bar, its properties match those indicated in previous studies, both in theory and observation. For example, all bars develop quickly in a few times 10^8 yr and have a length in the range from $\approx$4 to $\approx$8 kpc. We have also estimated the bar pattern rotation velocity to be around 30 km s^{-1} kpc^{-1} in general.

Concerning the vertical extent of bars, we show in Figure 11 that, as predicted, bars grow vertically thick as they evolve, producing a structure similar to a bulge seen edge-on and also presenting the characteristic boxy-peanut morphology. At the time this structure is present, the bar no longer belongs to the disk, since the growth in σ_z produces the vertically thick pseudobulge. Furthermore, our simulations indicate that this morphology develops quickly (in a few dynamical times, i.e., a few times 10^8 yr after the formation of the bar) and weakens after $\sim$1 Gyr. Thus, the boxy-peanut morphology may be used as an indication of a young bar, i.e., one that originated less than about 1 Gyr ago. Note also that the presence of a preexistent bulge would make it difficult to properly identify the boxy-peanut morphology.

However, in our simulations, σ_z in the bar does not exceed 50 km s^{-1} during the boxy-peanut phase and not even after 2 Gyr of bar evolution. This is shown in Figure 12, where we present the evolution in time of the stellar vertical velocity dispersion along the bar major and minor axes of our numerical experiment. These profiles were derived using the same procedures we used to produce the rotation curves discussed above. Although tentative, this is evidently in contrast to the observations we reported in the previous section, where evolved bars have $\sigma_z \sim 100$ km s^{-1}. Thus, while the processes that create the boxy-peanut morphology are fast, the one(s) responsible for the *observed* vertically thickening of the bars should happen on a longer timescale.

A qualitative analysis of Figure 12 proves very useful. In the first panel (at $t = 0$), corresponding to the initial conditions, the kinematics along major and minor axis of the disk should be (nearly) identical (with small differences from statistical fluctuations), as evolution has not yet started. To produce the velocity dispersion radial profile along the minor axis, we introduce an error of 5° in the slit position angle and an error in its central position of the order of a typical seeing measurement. This allows one to note that, indeed, the kinematics is similar in both axes and also to evaluate how these uncertainties, which are often present in real observations, would affect the measurements. At $t = 200$ the bar is recently formed and, as we argued above, keeps its kinematical properties along the vertical axis similar to those of the disk. At $t = 400$ and 600, however, the signature of the evolved bar is clear: in the region dominated by the bar (whose semimajor axis length is about 4 kpc), σ_z is substantially higher than in the bar-free region of the disk. Hence, our simulations give at least a qualitative support to the bar age diagnostic tool we introduced above. If bars are robust, they might keep this signature and yet possibly acquire higher values for σ_z, as we discuss in the next section. In our simulation, however, the bar weakened, a process that starts at $t = 800$ and continues until $t = 1000$, giving rise to an unbarred galaxy with a central morphologically bulgelike structure that also resembles bulges form the kinematical point of view.

For the typical distance of the galaxies in our sample ($cz \sim$ 1500 km s^{-1}) 10″ corresponds roughly to 1 kpc, which means that our spectroscopic measurements presented in § 4 go typically as far as about 2 kpc from the center, where our simulations

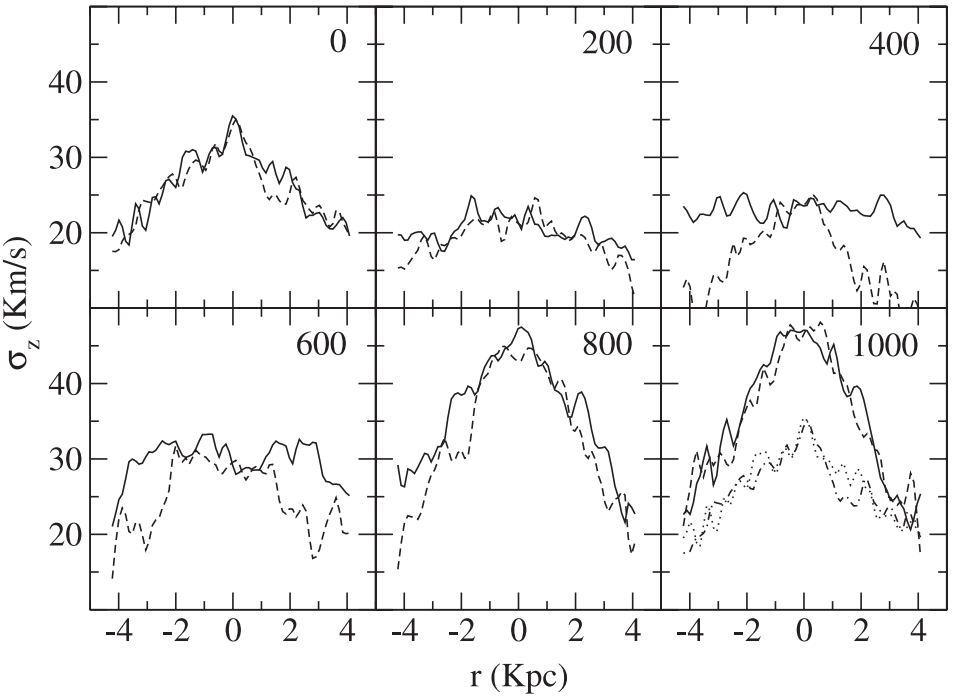

FIG. 12.—Radial profiles of the vertical velocity dispersion along the bar major axis (*solid line*) and minor axis (*dashed line*), as measured from simulated long-slit spectroscopy, in our representative stellar disk numerical simulation. The corresponding times in virial units are displayed in the top right of each panel. The last panel corresponds to 2 Gyr of evolution. In the last panel we plot the initial profiles again, as a dotted line for the major axis and as a dash-dotted line for the minor axis, for comparison.

(Fig. 12) show that a substantial difference in σ_z would be observed between the evolved bar and the disk.

6. DISCUSSION

The bar age diagnostic we present here allows us to distinguish between young and old bars, but a further question concerns knowing how large the age difference is. The results from the previous sections suggest that it is not only the processes causing the boxy-peanut morphology that produce bars as vertically thick as observed. This means that the age difference between young and old bars may be significantly in excess of 1 Gyr. We suggest now that another mechanism takes place during the evolution of the bar and that it continues after the vertical resonances and the hose instability end, giving the bar a vertical extent and a σ_z in agreement with what our observations show.

As shown by Spitzer & Schwarzschild (1951, 1953), collisions with giant molecular clouds (GMCs) can make the disk gradually hotter and vertically thicker. This is a process that happens in the disk as a whole (e.g., Binney 2001), but we can reasonably assume that these clouds may be more concentrated along the bar than in the rest of the disk, given that bars are indeed able to collect and funnel the gas present in the disk to the center. If this is true, then the effect of these collisions will be stronger in the bar region of the disk. It should also be mentioned that the same effect occurs as well with any other inhomogeneity in the stellar density distribution.

The variation in the stellar velocities provoked by the impact with GMCs may be written in the impulsive approximation as

$$(\Delta v)^2 = \left(\frac{2GM}{bv}\right)^2, \tag{16}$$

where M is the typical GMC mass and b is the impact parameter. The succession of several encounters gives origin to a process of diffusion in phase space (Wielen 1977) in the form

$$d\sigma_z^2 = D(\Delta v_z)\, dt, \tag{17}$$

where $D(\Delta v_z)$ is the diffusion coefficient (see Binney & Tremaine 1987), proportional to $(M/bv)^2$. If $D(\Delta v_z)$ is constant, then

$$\sigma_z^2 = \sigma_{0z}^2 + D(\Delta v_z)t, \tag{18}$$

where σ_{0z} is the initial vertical velocity dispersion. Through numerical simulations, Villumsen (1983) showed that the equation above may be parameterized in the form

$$\sigma_z = \sigma_{0z}\left(1 + \frac{t}{\tau}\right)^n, \tag{19}$$

with $n = \frac{1}{2}$ for a random walk diffusion and where τ is a timescale proportional to b^2/M^2. This value for n is in agreement with the relation between the velocity dispersion and the age of stars in the solar neighborhood.

Following the results from Villumsen (1983), this process may elevate the velocity dispersion from $\sigma_z \simeq 5$ to 25 km s^{-1} in about 7 Gyr. Assuming that GMCs are accumulated along the bar and since $\tau \propto b^2$, this mechanism may explain the observed vertical thickening of bars on timescales larger than 1 Gyr. If b along the bar is half the value of b in the remaining of the disk, resulting from a higher concentration of GMCs in the bar, then in 7 Gyr σ_z in the bar might go from $\sigma_z \simeq 5$ to 100 km s^{-1}, as observed.

If we consider that bars cease to be kinematically cold during the vertical thickening process, then we will have to take into account that the diffusion coefficient is not constant and that $d\sigma^2/dt \propto 1/\sigma$. This means that the scattering of stars by GMCs becomes less efficient over time as two kinematically distinct components form: the cold disk where GMCs fall and the vertically rising and hotter bar. This interpretation is certainly more justified from the theoretical point of view and leads to $n = \frac{1}{3}$, although the resulting differences are small. Following again the results from Villumsen (1983), this means that the bar takes more than an additional 1–2 Gyr to achieve $\sigma_z \simeq 100$ km s^{-1}.

The results from the simulations presented in Athanassoula (1992a, 1992b) and Patsis & Athanassoula (2000) may, however, represent a caveat to the analysis above. This is because they show that the gas concentrates in relatively narrow strips along the leading edges of bars. If GMCs behave like the gas in their simulations, then the consequences on the stellar dynamics within the bar may be different from what would be expected, if, as we assumed above, GMCs are uniformly distributed within the bar. One should note, however, that although dust lanes tend in fact to delineate strips along the leading edges of bars in real galaxies, there are also many examples of dust patches *across* bars (see, e.g., Sellwood & Wilkinson 1993).

It is worth noting at this point that in Paper II we measured the optical colors of bars in a sample of galaxies similar to the one in this work, including seven galaxies[5] studied here. We found that the average value for $B - V$ in the bars identified by our diagnostic as evolved is 1.1. In contrast, the identified young bars have $B - V$ equal to 0.7. This color difference can be translated to an age difference of the order of 10 Gyr (see, e.g., Tinsley & Gunn 1976; Maraston 1998), even allowing for reasonable differences in the metallicity of the stellar population. Although the age of the stellar population in the bar does not necessarily represent the age of the bar, this result, in agreement with what we found above with the numerical simulations, corroborates our suggestion that the age difference between young and old bars is significantly greater than 1 Gyr. Although here we are neglecting reddening by dust, this is justified by the fact that we defined the bar color at its ends where dust effects are minimized. There is also no reason to believe that dust attenuation should be more effective in galaxies with evolved bars than in those with recently formed bars. The reader is referred to Paper II for a more detailed discussion of these color comparisons. Interestingly, in this paper we also find that there are no significant differences in the photometric shape of young and old bars. In regard to the seven galaxies in common with the photometric analysis in Paper II, all of the bars show a flat surface brightness profile along the major axis, typical of barred galaxies with morphological types earlier than ≈Sbc (Elmegreen & Elmegreen 1985). Moreover, the elliptically averaged surface brightness radial profiles of the galaxies do not show any clear trend among young or old bars concerning profiles of Freeman types I and II (Freeman 1970).

According to this line of reasoning the evolved bars we identified in § 4 have ages not much less than the age of the universe and hence have neither dissolved at some time nor been recurrent. Obviously, this finding does not exclude the possibility of recurrent bars in other galaxies, but it does reinforce the results by Shen & Sellwood (2004), who suggest that bar dissolution requires much more mass concentration than observed and thus that bars are robust.

Using our diagnostic tool we showed in § 4 that from the 14 galaxies in our sample, 8 have evolved bars, whereas 5 have recently formed bars. This result may also be interpreted as observational evidence of the vertical thickening of bars. Evidently, a more direct way to evaluate the vertical structure of bars is to observe them in edge-on galaxies. In that case, however, the proper identification of bars remains difficult and also involves careful and detailed measurements. Furthermore, in edge-on galaxies it is impossible to retrieve several fundamental galactic properties and their detailed structural characteristics.

Our ability to estimate the ages of bars is an important step forward in the study of the formation and evolution of galaxies. We can, for instance, determine more precisely the timescales involved in the secular evolution processes related to bars and whether a given barred galaxy has already undergone them or not. In fact, we see that from the eight galaxies with evolved bars, only two (25%) have AGNs, whereas of the five galaxies with young bars, three (60%) show AGN activity. While this conclusion is still a matter of small-number statistics, it indicates that the timescale for the fueling of AGNs by bars is short. In that case, one may find a better correlation between the presence of bars and AGNs in galaxies when considering only young bars. This result is also corroborated by those from Paper II, which show that the average $B - I$ color in the bars of AGN galaxies is 1.7, while it is 2.1 in galaxies without nuclear activity. One word of caution, however: the significance of these results is debatable, since AGN classifications are derived by different authors in different ways.

It is also interesting to note that of the eight evolved bars, seven (88%) reside in early-type galaxies (S0–Sa), while only one (12%) is in an Sb galaxy. On the contrary, the young bars seem to preferentially inhabit later type galaxies: of the five young bars, two (40%) are found in S0–Sa galaxies and three (60%) in Sb galaxies. This point is further explored in Paper II. It is also important to stress once again that these results must be confirmed by studies with much larger samples, since the small number statistics involved here means their statistical significance is low.

7. CONCLUSION

By exploring the predicted vertical thickening of bars during their evolution through measurements of the vertical kinematics, made along the bars' major and minor axes in a sample of 14 galaxies, we have developed and introduced a diagnostic tool that allows us to distinguish between recently formed and evolved bars. Using several *N*-body realizations of bar unstable disk galaxies, we studied the timescale involved in the vertical evolution of bars and the conditions necessary to the onset of the bar instability.

We found that bars may be broadly distributed between young and old bars by essentially comparing the vertical velocity dispersion in the bar and in the disk in which it formed. Young bars are kinematically similar (in the vertical direction) to the disks they reside in, having a low vertical velocity dispersion, and thus remaining a vertically thin structure in the disk. Old bars, however, have values for vertical velocity dispersion significantly higher than those in their disks and hence form a vertically thick structure that does no longer belongs to the disk.

We present evidences that the timescale for the vertical thickening of bars may be substantially larger than 1 Gyr and thus that another physical process in addition to the vertical

[5] These are NGC 4314, NGC 4394, NGC 4579, NGC 4608, NGC 5383, NGC 5701, and NGC 5850—i.e., the north sample—which give us three recently formed bars and four evolved ones.

resonances and the hose instability may be also playing a major role in this context. The evidence for this conclusion comes, first, from the numerical experiments, which show that even after 2 Gyr of evolution, the simulated bars have a vertical velocity dispersion that does not exceed 50 km s^{-1}, whereas in our observed bars we have measured values of the order of 100 km s^{-1}. Second, this result is corroborated by those we present in Paper II, showing that the average color difference between vertically thin and thick bars suggests an age difference of about 10 Gyr. These results reinforce our suggestion that the Spitzer-Schwarzchild mechanism is responsible for the later vertical thickening of bars, since we demonstrated that it can produce the observed values for the vertical velocity dispersion in these longer timescales. Furthermore, our simulations also show that the boxy-peanut morphology appears quickly, in a few dynamical times after the formation of the bar, and also dissolves relatively quickly, after about 1 Gyr, thus representing an indication of a recently formed bar.

Estimating the ages of bars is clearly an important goal in the study of the formation and evolution of galaxies, as it has been proved many times now the major role bars play in this matter. In this paper, we show how age estimations can help us better understand the intricate relationship between bars and the fueling of AGNs. In Paper II, we use this tool, together with multiband imaging data, to explore further the impact of the formation and evolution of bars on the formation and evolution of galaxies. It is highly desirable now to obtain high-quality kinematical data along bars in an increasing number of galaxies and also to try to extend them to the outer bar and disk limits, especially to avoid the effects of a bulge. While we are now able to distinguish bars that are recently formed from the ones that have been already evolving for timescales of several gigayears, the next relevant step is to develop a theoretical understanding of the processes involved in the vertical evolution of bars in order to be able to refine these age estimates.

This work was financially supported by FAPESP grants 99/07492-7, 00/06695-0, and 98/10138-8. We thank Rob Kennicutt for his kind hospitality during a visit to the Steward Observatory, where part of this work was undertaken. It is a pleasure to thank Lia Athanassoula for her detailed reading and comments on a first version of this manuscript, in particular on its theoretical aspects, which helped to improve our work. Comments and suggestions from both the observational and theoretical anonymous referees were invaluable and helped to substantially improve the presentation of our results. We would like to thank Peter Teuben for help on using NEMO (http://bima.astro.umd.edu/nemo/). This research has made use of Aladin and of the NASA/IPAC Extragalactic Database (NED), which is operated by the Jet Propulsion Laboratory, California Institute of Technology, under contract with the National Aeronautics and Space Administration. This research has also made use of NASA's Astrophysics Data System, the Lyon Extragalactic Data Archive (LEDA; http://leda.univ-lyon1.fr/), and of spectral data retrieved from the Elodie archive at the Observatoire de Haute-Provence (OHP; http://atlas.obs-hp.fr/elodie). Statistical tests were made within the R environment (http://www.R-project.org).

REFERENCES

Abramowitz, M., & Stegun, I. A. 1965, Handbook of Mathematical Functions with Formulas, Graphs, and Mathematical Tables (New York: Dover)
Abt, H. A., & Biggs, E. S. 1972, Bibliography of Stellar Radial Velocities (New York: Latham)
Athanassoula, E. 1992a, MNRAS, 259, 328
———. 1992b, MNRAS, 259, 345
———. 2002, ApJ, 569, L83
———. 2003, MNRAS, 341, 1179
Athanassoula, E., & Bureau, M. 1999, ApJ, 522, 699
Athanassoula, E., Fady, E., Lambert, J. C., & Bosma, A. 2000, MNRAS, 314, 475
Athanassoula, E., & Misiriotis, A. 2002, MNRAS, 330, 35
Balcells, M., & Peletier, R. F. 1994, AJ, 107, 135
Barnes, E. I., Sellwood, J. A., & Kosowsky, A. 2004, AJ, 128, 2724
Barnes, J., & Hut, P. 1986, Nature, 324, 446
Berentzen, I., Heller, C. H., Shlosman, I., & Fricke, K. J. 1998, MNRAS, 300, 49
Binney, J. 2001, in ASP Conf. Ser. 230, Galaxy Disks and Disk Galaxies, ed. J. G. Funes, S. J. Corsini, & E. M. Corsini (San Francisco: ASP), 63
Binney, J., & Merrifield, M. 1998, Galactic Astronomy (Princeton: Princeton Univ. Press)
Binney, J., & Tremaine, S. 1987, Galactic Dynamics (Princeton: Princeton Univ. Press)
Blitz, L., & Spergel, D. N. 1991, ApJ, 379, 631
Bonnarel, F., et al. 2000, A&AS, 143, 33
Bottema, R. 1993, A&A, 275, 16
Bournaud, F., & Combes, F. 2002, A&A, 392, 83
Bureau, M., & Athanassoula, E. 1999, ApJ, 522, 686
———. 2005, ApJ, 626, 159
Bureau, M., & Freeman, K. C. 1999, AJ, 118, 126
Buta, R. 1986, ApJS, 61, 609
Buta, R., & Combes, F. 1996, Fundam. Cosmic Phys., 17, 95
Carollo, C. M., Stiavelli, M., de Zeeuw, P. T., & Mack, J. 1997, AJ, 114, 2366
Cayrel de Strobel, G., Soubiran C., & Ralite N. 2001, A&A, 373, 159
Chung, A., & Bureau, M. 2004, AJ, 127, 3192
Combes, F., Debbasch, F., Friedli, D., & Pfenniger, D. 1990, A&A, 233, 82
Combes, F., & Gerin, M. 1985, A&A, 150, 327
Combes, F., & Sanders, R. H. 1981, A&A, 96, 164
Corsini, E. M., Pizzella, A., Coccato, L., & Bertola, F. 2003, A&A, 408, 873
Courteau, S., de Jong, R. S., & Broeils, A. H. 1996, ApJ, 457, L73
Crenshaw, D. M., Kraemer, S. B., & Gabel, J. R. 2003, AJ, 126, 1690
Debattista, V. P., Carollo, C. M., Mayer, L., & Moore, B. 2004, ApJ, 604, L93
de Grijs, R., & Peletier, R. F. 1997, A&A, 320, L21
Dehnen, W., & Binney, J. J. 1998, MNRAS, 298, 387
Delhaye, J. 1965, Galactic Structure, ed. A. Blaauw & M. Schmidt (Chicago: Univ. Chicago Press)
de Souza, R. E., & dos Anjos, S. 1987, A&AS, 70, 465
de Souza, R. E., Gadotti, D. A., & dos Anjos, S. 2004, ApJS, 153, 411
de Vaucouleurs, G., de Vaucouleurs, A., Corwin, H. G., Jr., Buta, R. J., Paturel, G., & Fouqué, P. 1991, Third Reference Catalog of Bright Galaxies (New York: Springer) (RC3)
Edvardsson, B., Andersen, J., Gustafsson, B., Lambert, D. L., Nissen, P. E., & Tomkin, J. 1993, A&A, 275, 101
Elmegreen, B. G., & Elmegreen, D. M. 1985, ApJ, 288, 438
Elmegreen, B. G., Elmegreen, D. M., & Hirst, A. C. 2004, ApJ, 612, 191
Emsellem, E., Greusard, D., Combes, F., Friedli, D., Leon, S., Pécontal, E., & Wozniak, H. 2001, A&A, 368, 52
Fisher, D. 1997, AJ, 113, 950
Freeman, K. C. 1970, ApJ, 160, 811
———. 1978, in IAU Symp. 77, Structure and Properties of Nearby Galaxies, ed. E. M. Berkhuijsen & R. Wielebinski (Dordrecht: Reidel), 3
Friedli, D., & Benz, W. 1993, A&A, 268, 65
———. 1995, A&A, 301, 649
Gadotti, D. A., & de Souza, R. E. 2003, ApJ, 583, L75
———. 2005, ApJ, submitted (Paper II)
Gadotti, D. A., & dos Anjos, S. 2001, AJ, 122, 1298
Gerssen, J., Kuijken, K., & Merrifield, M. R. 1997, MNRAS, 288, 618
———. 2000, MNRAS, 317, 545
Goudfrooij, P., & Emsellem, E. 1996, A&A, 306, L45
Ho, L. C., Filippenko, A. V., & Sargent, W. L. W. 1997a, ApJ, 487, 579
———. 1997b, ApJ, 487, 591
Hoffleit, D., & Warren, W. H. 1995, The Bright Star Catalogue (5th ed.; New Haven: Yale Univ. Obs.)
Jogee, S., et al. 2004, ApJ, 615, L105
Jungwiert, B., Combes, F., & Axon, D. J. 1997, A&AS, 125, 479
Kalnajs, A. J. 1972, ApJ, 175, 63
Kennicutt, R. C. 1992, ApJS, 79, 255
Knapen, J. H., Shlosman, I., & Peletier, R. F. 2000, ApJ, 529, 93
Kormendy, J. 1982, ApJ, 257, 75
Kormendy, J., & Illingworth, G. 1983, ApJ, 265, 632

Kormendy, J., & Kennicutt, R. C. 2004, ARA&A, 42, 603
Kregel, M., van der Kruit, P. C., & Freeman, K. C. 2004, MNRAS, 351, 1247
Kuijken, K., & Merrifield, M. R. 1995, ApJ, 443, L13
Laine, S., Shlosman, I., Knapen, J. H., & Peletier, R. F. 2002, ApJ, 567, 97
Laurikainen, E., Salo, H., & Buta, R. 2004, ApJ, 607, 103
Maraston, C. 1998, MNRAS, 300, 872
Martin, P., & Roy, J. R. 1994, ApJ, 424, 599
Massey, P. 1997, A User's Guide to CCD Reductions with IRAF (Tucson: NOAO), http://iraf.noao.edu/docs/spectra.html
Massey, P., Valdes, F., & Barnes, J. 1992, A User's Guide to Reducing Slit Spectra with IRAF (Tucson: NOAO), http://iraf.noao.edu/docs/spectra.html
McElroy, D. B. 1995, ApJS, 100, 105
Merrifield, M. R. 2004, in ASP Conf. Ser. 317, Milky Way Surveys: The Structure and Evolution of our Galaxy, ed. D. Clemens, R. Shah, & T. Brainerd (San Francisco: ASP), 298
Merrifield, M. R., & Kuijken, K. 1999, A&A, 345, L47
Merritt, D. 1996, AJ, 111, 2462
Merritt, D., & Sellwood, J. A. 1994, ApJ, 425, 551
Mulchaey, J. S., & Regan, M. W. 1997, ApJ, 482, L135
Noguchi, M. 2000, MNRAS, 312, 194
Norman, C. A., Sellwood, J. A., & Hasan, H. 1996, ApJ, 462, 114
Oke, J. B. 1990, AJ, 99, 1621
Patsis, P. A., & Athanassoula, E. 2000, A&A, 358, 45
Peletier, R. F., & Balcells, M. 1996, AJ, 111, 2238
Pfenniger, D., & Norman, C. 1990, ApJ, 363, 391
Pizzella, A., Corsini, E. M., Vega Beltrán, J. C., & Bertola, F. 2004, A&A, 424, 447
Polyachenko, V. L., & Polyachenko, E. V. 2003, Astron. Lett., 29, 447
Prugniel, Ph., & Soubiran, C. 2001, A&A, 369, 1048
Rix, H.-W., & White, S. D. M. 1992, MNRAS, 254, 389
Rubin, V. C., Burstein, D., Ford, W. K., & Thonnard, N. 1985, ApJ, 289, 81
Sakamoto, K., Okumura, S. K., Ishizuki, S., & Scoville, N. Z. 1999a, ApJ, 525, 691
———. 1999b, ApJS, 124, 403
Sandage, A., & Bedke, J. 1994, The Carnegie Atlas of Galaxies, Vol. 1 (Washington: Carnegie Inst.)
Schwarz, M. P. 1981, ApJ, 247, 77
Sellwood, J. A., & Moore, E. M. 1999, ApJ, 510, 125
Sellwood, J. A., & Wilkinson, A. 1993, Rep. Prog. Phys., 56, 173
Sérsic, J. L., & Pastoriza, M. 1965, PASP, 77, 287
———. 1967, PASP, 79, 152
Shen, J., & Sellwood, J. A. 2004, ApJ, 604, 614
Sheth, K., Regan, M. W., Scoville, N. Z., & Strubbe, L. E. 2003, ApJ, 592, L13
Shlosman, I., Begelman, M. C., & Frank, J. 1990, Nature, 345, 679
Shlosman, I., Frank, J., & Begelman, M. C. 1989, Nature, 338, 45
Spitzer, L., & Schwarzschild, M. 1951, ApJ, 114, 385
———. 1953, ApJ, 118, 106
Teuben, P. J. 1995, in ASP Conf. Ser. 77, Astronomical Data Analysis Software and Systems IV, ed. R. A. Shaw, H. E. Payne, & J. J. E. Hayes (San Francisco: ASP), 398
Tinsley, B. M., & Gunn, J. E. 1976, ApJ, 203, 52
Tonry, J., & Davis, M. 1979, AJ, 84, 1511
Toomre, A. 1963, ApJ, 138, 385
———. 1964, ApJ, 139, 1217
———. 1966, Notes on the 1966 Summer Study Program in Geophysical Fluid Dynamics at Woods Hole Oceanographic Institution, Vol. 1 (Woods Hole: Woods Hole Oceanographic Inst.), 111
———. 1981, Structure and Evolution of Normal Galaxies, ed. S. M. Fall & D. Lynden-Bell (Cambridge: Cambridge Univ. Press), 111
van den Bergh, S. 2002, AJ, 124, 782
van der Kruit, P. C. 2002, in ASP Conf. Ser. 273, The Dynamics, Structure, and History of Galaxies, ed. G. S. Da Costa & Helmut Jerjen (San Francisco: ASP), 7
van der Kruit, P. C., & Searle, L. 1981, A&A, 95, 105
van der Marel, R. P., & Franx, M. 1993, ApJ, 407, 525
Villumsen, J. V. 1983, ApJ, 274, 632
Wielen, R. 1977, A&A, 60, 263
Zaritsky, D., Kennicutt, R. C., & Huchra, J. P. 1994, ApJ, 420, 87